UNIVERSITÀ DEGLI STUDI DI PADOVA

DIPARTIMENTO DI INGEGNERIA INDUSTRIALE

CORSO DI LAUREA IN INGEGNERIA DEI MATERIALI

Tesi di Laurea in

Ingegneria dei Materiali

MECHANICAL PROPERTIES OF HYDROGELS FOR PILLARS FABRICATION AND BIOLOGICAL APPLICATIONS

Relatore: Prof. Giovanna Brusatin

Correlatore: Dott. Gioia della Giustina

Laureando: UMBERTO PAGGI

ANNO ACCADEMICO 2016 – 2017

Abstract

In questa testi si è studiato il comportamento meccanico di hydrogel a base di polietilenglicolediacrilato e poliacrilammide a diverse concentrazioni, dal 5% al 60%; i campioni sono stati misurati con compressione a piatti paralleli, macro indentazione con punta sferica e micro indentazione a punta piramidale per testare la diversa risposta del materiale in esame a sollecitazioni macroscopiche e microscopiche.
Vista la discrepanza tra i valori ottenuti nei due casi, si è formulata un'ipotesi che tenga in considerazione del rilassamento poroelastico del materiale: per calcolare la costante di diffusione di materia dei singoli campioni è stata quindi fatta una misura di rilassamento dello sforzo mediante compressione a piatti paralleli.
Gli hydrogel così caratterizzati sono stati impiegati per la produzione di substrati microstrutturati con geometria a pillars su cui è stata fatta una cultura di cellule staminali embrionali umane.

In this study we have characterised the mechanical behaviour of polyethilenglycolediacrylate and polyacrylamide based hydrogels with varying concentrations, from 5% up to 60%; samples were measured with parallel plates compression, macro indentation with spherical indenter and micro indentation with pyramidal indenter to test different response of the studied material to macroscopic and microscopic solicitations.
Due to the discrepancy between values obtained in the two cases, an hypothesis was formulated which accounts for poroelastic relaxation of the material: to calculate the mass diffusion constant of single samples hence a stress relaxation measure was performed with parallel plates compression.
Hydrogels characterised in this way were employed for the production of microstructurated substrates with pillar geometry on which human embryonic stem cells were cultured.

Index

Chapter 1

Introduction

Gels are defined as a substantially dilute cross-linked system, which exhibits no flow when in the steady-state. By weight, gels are mostly liquid, yet they behave like solids due to a three-dimensional cross-linked network: this internal network structure may result from physical bonds (physical gels) or chemical bonds (chemical gels), as well as crystallites or other junctions that remain intact within the extending fluid. The ability of hydrogels to absorb water derives from functional groups attached to the polymeric backbone, while their resistance to dissolution relies on cross-links between network chains and physical entanglements; many materials, both naturally occurring and synthetic, fit the definition of hydrogels.

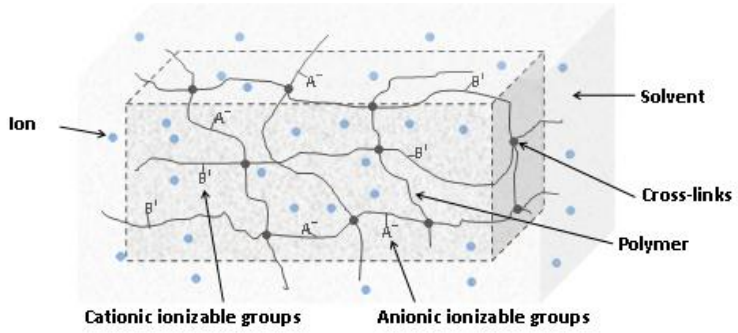

Fig.1: General structure of a hydrogel.

An interesting aspect of these materials, particularly striking for synthetic hydrogels, is the possibility of tuning they mechanical and transport properties in many ways that range from simply changing their concentration [1, 2, 4, 7] to increasingly complex fashions such as varying their composition [2, 3, 5, 11] or adjusting their crosslinking degree [1, 4, 6, 7, 8] and finally altering its solvent or the solutes in it [2, 7, 9, 10] with the possibility to obtain a material that behaves in a way or the other in relation to its environment. These features make hydrogels an ideal choice for biological studies, since we can recreate in vitro a situation typical of the in vivo physical environment of a cell, and vary one aspect at a time to investigate their effect on the subject being researched.

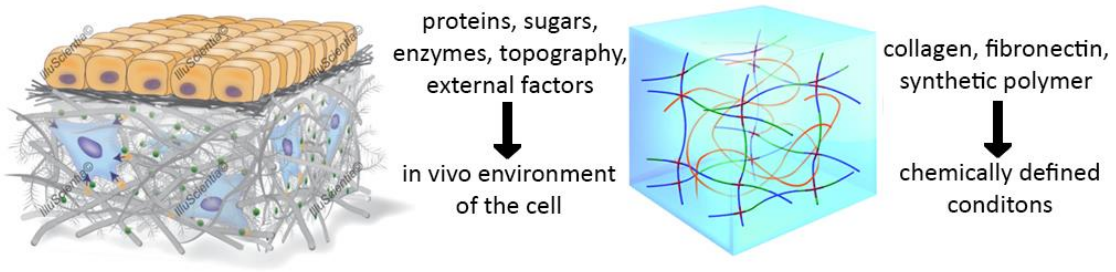

Fig.2: A living cell is in immersed in a complex and always changing environment, while hydrogel gives a well known, stable substrate with tuneable properties.

For this study in particular we will focus on determining the stiffness of hydrogels with different concentrations both on the macroscale but more importantly on the microscale: recent studies have shown that cells perceive their surroundings not only predominantly through chemical interactions as it was previously thought, but indeed a consistent role in cell differentiation is played by the elastic modulus of the environment around them [32, 33, 34, 35]. It is hence crucial to understand how matrixes behaves and respond locally contrary to the standard macro determination of mechanical properties.

Chapter 2

State of the art

2.1 Mechanical properties of hydrogels

Polymers' mechanical behaviour may vary widely based on chemical structure and composition, presence of solvents or additives, temperature and the application time of the stress involved: the last one in particular is fundamental since polymers, which deformations are regulated by entropic forces, depend strongly from molecular mobility and relaxation times.
This characteristic distinguishes polymeric materials from all the others and is the origin of rubber elasticity and viscoelastic behaviour which is often encountered when working with hydrogels, and that occurs at temperatures around the glass transition at which the response is not glassy nor rubbery, but indeed viscoelastic.

2.1.1 Rubber elasticity

Normal rubbers are lightly cross-linked networks with a rather large free volume that allows them to respond to external stresses with a rapid rearrangement of the polymer segments. In their swollen state, most hydrogels satisfy these criteria for a rubber: the macromolecular network structure of elastomeric materials enables these materials to undergo large strain, nonlinear elastic deformations; the underlying structure is essentially one of randomly oriented, long chain molecules in a network arrangement due to sparse cross-linking between the long molecules with weak intermolecular interactions between one another.
The nature of this structure results in a stress–strain behaviour that is primarily governed by changes in configurational entropy as the randomly-oriented molecular network becomes preferentially-oriented with stretching. We can express its equation state as

$$F = \left(\partial U/\partial L\right)_{T;V} + T\left(\partial F/\partial T\right)_{L;V}$$

where F is the retractive force of the elastomer in response to a tensile force, U is the internal energy, L is the length, V is the volume, and T is the temperature.

For what was said, however, the first term of the equation is equal to zero, since bonds are not stretched by the bulk elongation and so the internal energy is constant, contrary to what usually happens in materials like metals in which the bond length increases storing the elastic energy, for that are indeed called "enthalpic materials".

Due to the alignment of chains with the stress follows a more orderly system and consequentially a decrease in entropy, so all considered the previous equation becomes

$$\left(\partial U/\partial L\right)_{T;V} = 0 \quad \text{and} \quad \left(\partial F/\partial T\right)_{L;V} = -\left(\partial S/\partial L\right)_{T;V}$$

$$F = -T\left(\partial S/\partial L\right)_{T;V} = -KT\left(\partial ln\Omega(r,T)/\partial r\right)_{T;V}$$

where S is entropy, K is the Boltzmann constant, r is a certain end-to-end distance of polymeric chains, and Ω(r,T) is the probability that the polymeric chains with an end-to-end distance r at temperature T will adopt a certain conformation. The last form of the equation derives from statistical thermodynamics.

This theoretical explanation doesn't perfectly match the experimental data: in fact, as the polymer chain unwinds and extend its interaction with surrounding chains becomes more and more relevant; at deformations where r begins to approach its maximum value (that is, around 40% of the total unwinded length), the non-Gaussian nature of the chain stretch must be taken into account. To incorporate these more accurate individual chain statistics into a constitutive framework, it is necessary to have a model that links the stretch of individual chains to the applied

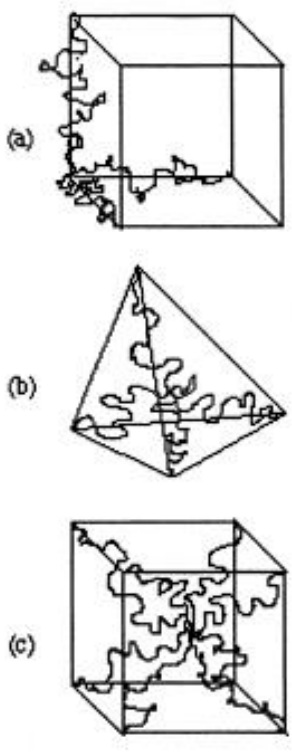

Fig.3: Unit cells of the representative network structure: 3-chains model (a), 4-chains model (b) and 8-chains model (c)[2].

deformation: this is accomplished by assuming a representative network structure in which every crosslinking point is associated with a unit cell and is taken to deform in principal stretch space. They are considered to be incompressible and differ in how the deformation of the chains is related to the deformation of the cell, which varies from the simplest 3-chain model to the most complex 8-chain.
In the first one the chains are located along the axes of the cubic cell and aligned with the principal stress directions, so it predicts well just the uniaxial behaviour since considers only the response of the chain parallel to the force applied and ignores the network response of the underlying structure.
A second one was proposed, the 4-chains model, with a higher degree of cooperation but even if it performed better it didn't predict well enough complex stress states.
At last the 8-chains model was theorised which gave the best fitting of experimental data, with the chains located along the diagonals that undergo tensile stretching for all imposed deformations, mimicking what would be expected in the cooperative deformation of a real network.
It was also noted that for the low stretch region the Gaussian model could be implemented, since it predicted the rubbery behaviour the worse the more complex the stress state is, so the Flory-Erman model was produced which factor in the interaction between chains as a constrain factor that influences the crosslinks junctions.

Even with this complex models, the biaxial fitting of the 8-chains was not satisfactory, and that's because it capture the limits behind maximum extensibility of a chain, but not what happens before that point is reached; the natural next step is therefore to join the Flory-Erman model for chain interaction and low extension with the stretch limit, network behaviour 8-chains model, with satisfactory results.
These theory, although mathematically convoluted, rely on very few physical parameters and have in that their simplicity; moreover by the fitting of experimental data one could retrieve useful information, the most studied of which is the mean molecular weight between crosslinks, which is directly connected to mechanical and swelling properties.
These aspects however, and a detailed mathematical dissertation of what have been said to this point, are beyond the purpose of this thesis and are left to the articles cited. [1, 22]

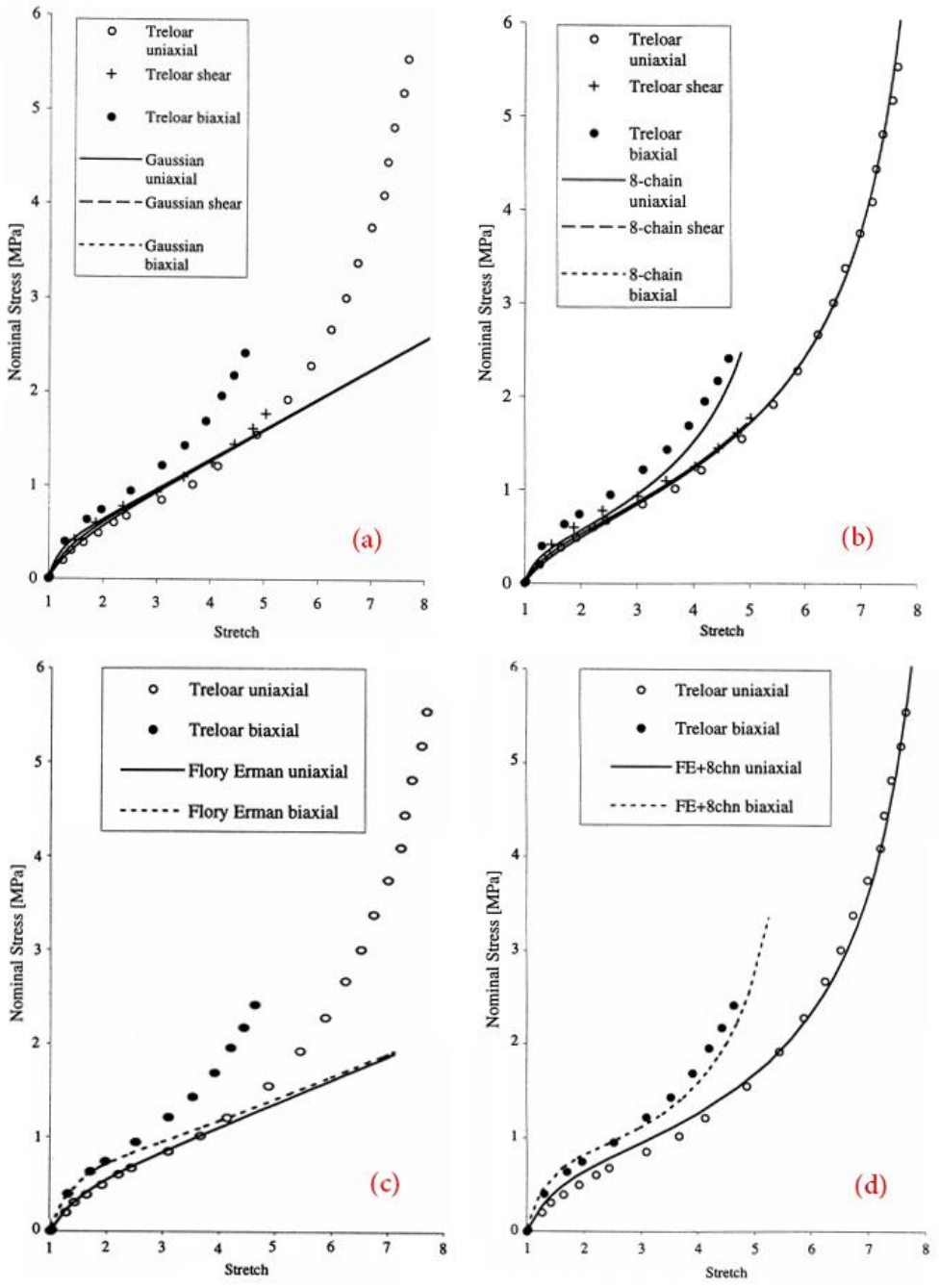

Fig.4: Different model for analysing the rubber elasticity: (a)Gaussian statistic model which is a fair approximation of the experimental data at low stress, (b) "8-chains" model that predicts very well the uniaxial behaviour but doesn't account completely for chain interaction in more complex scenarios, (c) a better fitting of the low stress region with the Flory-Erman model and finally (d) the complete Flory-Erman + 8-chains model capable of explaining the rubbery behaviour at low and high elongation for every stress configuration [2].

2.1.2 Viscoelasticity

What is at the base of this property is molecular relaxation: a viscoelastic deformation of a polymeric material causes a modification of its macromolecules conformation and possibly of their relative position; at the stress removal, these chains tend to return partially at their initial condition, but for this to be possible a given relaxation time is required.
To describe this behaviour we'll suppose that to be the combination of two different components, one elastic and one viscous, which deformations are described by Hooke and Newton laws

$\sigma = E\varepsilon$ or $\mathrm{d}\sigma/\mathrm{d}t = E\ \mathrm{d}\varepsilon/\mathrm{d}t$ Hooke law

$\sigma = \eta\ \mathrm{d}\varepsilon/\mathrm{d}t$ Newton law

2.1.2.1 Maxwell model for stress relaxation

It is idealised as a spring and a piston, when a load is applied the resulting deformation is the sum of the elastic and viscous one, while the strain on the two element is equal:

$\varepsilon = \varepsilon_E + \varepsilon_V$ or $\mathrm{d}\varepsilon/\mathrm{d}t = \mathrm{d}\varepsilon_E/\mathrm{d}t + \mathrm{d}\varepsilon_V/\mathrm{d}t$

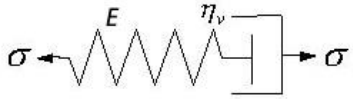

Fig.5: Maxwell model

considering the previous Hooke and Newton equations

$\mathrm{d}\sigma/\mathrm{d}t = E\ \mathrm{d}\varepsilon_E/\mathrm{d}t$ and $\sigma = \eta\ \mathrm{d}\varepsilon_V/\mathrm{d}t$

so we have $\mathrm{d}\varepsilon/\mathrm{d}t = \mathrm{d}\sigma/\mathrm{d}t\ 1/E + \sigma/\eta$

Since we want to predict the stress relaxation, in which a constant ε is imposed and the strain is measured, the equation can be simplified

$0 = \mathrm{d}\sigma/\mathrm{d}t\ 1/E + \sigma/\eta$ from which $\mathrm{d}\sigma/\sigma = \mathrm{E}\mathrm{d}t/\eta$

Integrating the last one we obtain

$$\sigma = \sigma_0 e^{-\left(Et/\eta\right)} = \sigma_0 e^{-(t/\tau_0)} = \sigma(t) \quad \text{from which} \quad G(t) = {}^{\sigma(t)}/_{\varepsilon_0}$$

Where τ_0 is the relaxation time, and G(t) is the relaxation modulus, which is a valid definition only in the case of linear viscoelastic behaviour that is true at low stresses. In figure 2 (left) is shown that two different G(t) exist, one in the unrelaxed stress region and the second in the relaxed stress region. This trend is not well fitted by the Maxwell model (red line), indeed a better representation of experimental data is obtained with the Maxwell-Wiechert model which combine more Maxwell's elements together (green line).

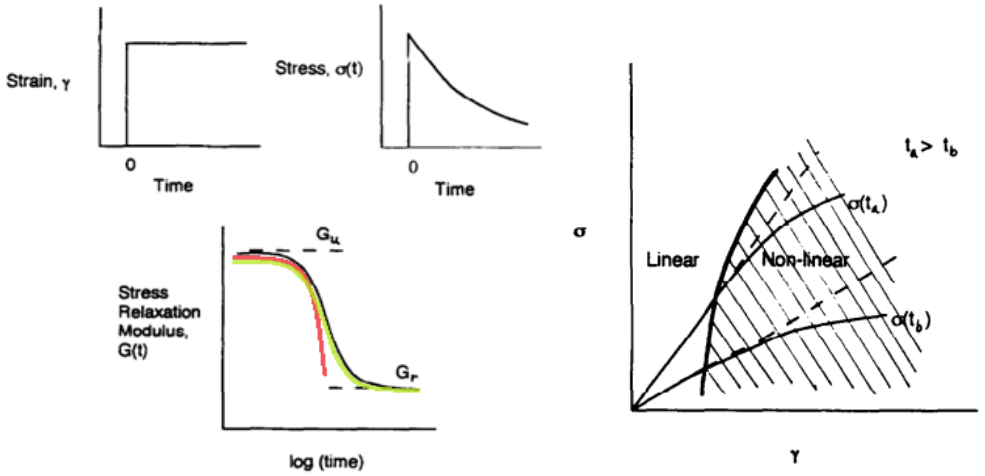

Fig.6: Stress relaxation: (left) a constant strain applied at t = 0 leads to a time-dependent stress. G_u, and G_r, are the unrelaxed and relaxed stress relaxation moduli with the Maxwell model approximation (red) and the Maxwell-Wiechert model (green).
From several isochronal stress-strain plots (right), the regions of linear and nonlinear viscoelastic behaviour are identified. This plot is not obtained from a conventional stress-strain test, but the data are taken from several stress relaxation experiments at different strains [1]

2.1.2.2 Kelvin-Voigt model for creep

The elements are the same of the Maxwell model, but arranged in parallel; with this setup the elongation is the same in the two elements, but the stress is divided between the two

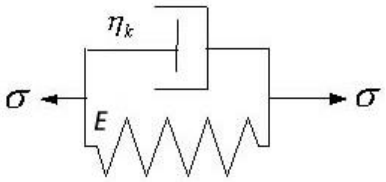

Fig.7: Kelvin-Voigt model

$$\sigma = \sigma_E + \sigma_V$$

For the first term we apply the Hooke law, while for the second the Newton's is valid, thus obtaining

$$d\varepsilon/dt = \sigma/\eta - E\varepsilon/\eta \quad \text{or otherwise} \quad d\varepsilon/dt + E\varepsilon/\eta = \sigma/\eta$$

which is a differential equation that integrated gives

$$\varepsilon = \sigma_0/E\left[1 - e^{-\left(Et/\eta\right)}\right] = \sigma_0/E\left[1 - e^{-\left(t/\tau_0\right)}\right] = \varepsilon(t) \quad \text{from which} \quad J(t) = \varepsilon(t)/\sigma_0$$

In this case τ_0 is called delay time and J(t) is the compliance, which is still valid only in the linear viscoelastic behaviour region that is at low intensity load. Again we found that two different compliances exist, one for the unrelaxed region and the relaxed region, and also that compliance and stress relaxation modulus can be correlated as follow, but only outside of the transition zone that is when the two properties are almost time independent.

$$G(t) = 1/J(t)$$

One again, we can use the Maxwell-Wiechert model by placing multiple Kelvin-Voigt elements in series, and the resulting system will have a better approximation of the experimental data of the compliance.

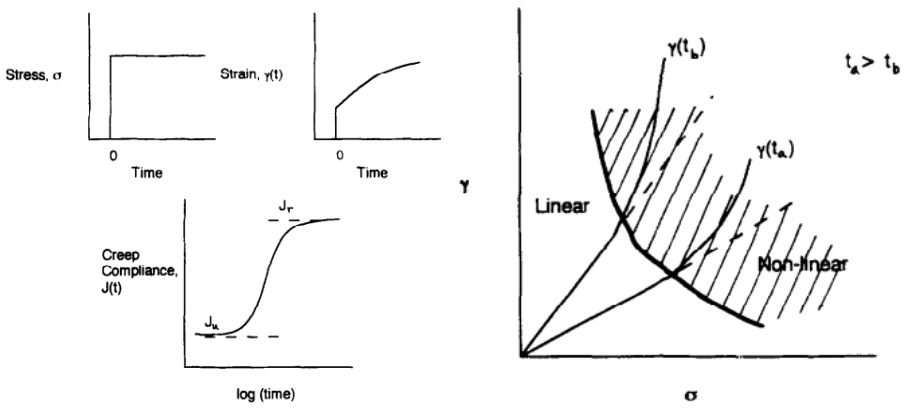

Fig.8: Creep: (left) a constant stress applied at t = 0 leads to a time-dependent strain. J_u, and J_r, are the unrelaxed and relaxed compliances.
From several isochronal strain-stress plots, the regions of linear and nonlinear viscoelastic behaviour are identified. This plot is not obtained from a conventional stress-strain test, but the data art taken from several creep experiments at different stresses [1].

2.1.2.3 Poroelasticity

In hydrogels, the time dependent deformation is the result of two concurrent molecular processes: the conformational change of the network explained above with the Maxwell model, and the migration of the solvent molecules; when the network is under load the solvent present between its chains feels a pressure gradient which causes molecules to migrate from high stress to lower stress region. At a macroscopic scale, the two processes result in viscoelastic and poroelastic deformation respectively.

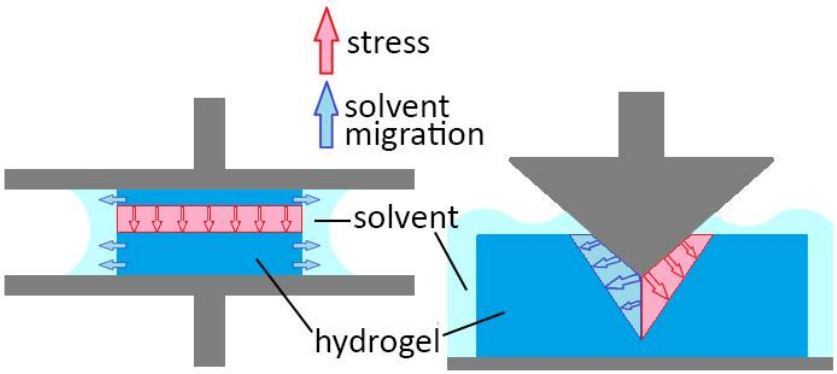

Fig.9: Pressure gradient in a hydrogel in a standard compression test and in an indentation measurement; in the first case we have an homogeneous stress field which causes solvent to flow out of the sample, while the indentation creates a complex field inside the sample which causes solvent to migrate remaining inside the hydrogel.

Typically these phenomena are studied through a compression test, and it is interesting to notice that as long as the mesh size of the network is much smaller than the contact size of the probe, the viscoelastic relaxation time is independent of the contact size of the probe, while the poroelastic relaxation time is quadratic in this parameter, therefore, the two types of deformation can be differentiated. The curves obtained are similar to the ones seen above for simple viscoelastic relaxation and can be interpreted again with the Maxwell model, this time however we'll get two relaxation times, τ_p for the poroelastic deformation and τ_v for the viscoelastic one [37, 38, 39, 40].

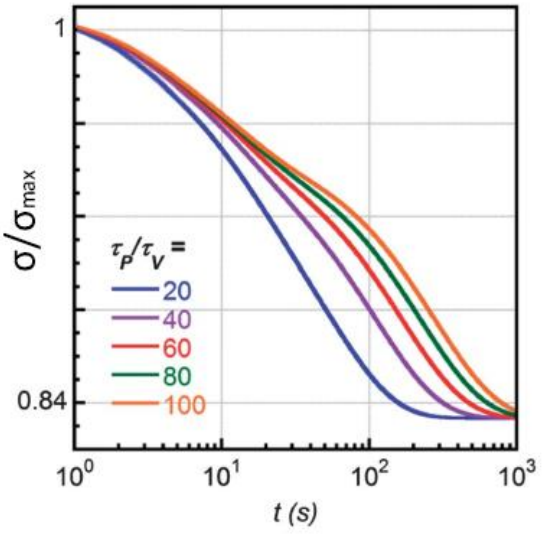

Fig.10: Theoretical prediction of hydrogel relaxation for several τ_p vs τ_v ratios. At high enough τ_p we can assume the relaxation to be only poroelastic [40].

2.1.3 Dynamic response

Dynamic mechanical analysis provides quantitative information on the viscoelastic and rheological properties of a material by measuring the mechanical response of a sample as it is deformed under periodic stress (or strain). The most common setup is to apply a shear stress and measure the dynamic shear modulus G*, but similar definitions can be applied for testing axial deformation and the dynamic Young's modulus E*, and so on.
Upon a sinusoidal stress of angular frequency ω it is measured the response of the sample, that is its deformation as a function of ω: if the material was perfectly elastic the feedback would be instantaneous and in phase with the stimulus

$$\tau(t) = \tau_0 \sin(\omega t) = G\gamma_0 \sin(\omega t)$$
$$\gamma(t) = \gamma_0 \sin(\omega t)$$

while for a Newtonian fluid there would be a 90° offset

$$\tau(t) = \eta\gamma(t) = \eta \, {}^{\mathrm{d}}/_{\mathrm{d}t} \, (\gamma_0 \sin(\omega t)) = \eta\gamma_0 \, \omega\cos(\omega t)$$

Thus, for a viscoelastic material an offset angel between 0° and 90° is predicted, which is related to the energy dissipation due to the viscous behaviour. Therefore, under an alternating, sinusoidal stress the feedback of said material is expected to have an offset δ and its expressions are

$$\tau(t) = \tau_0 \sin(\omega t + \delta)$$
$$\gamma(t) = \gamma_0 \sin(\omega t)$$

From the stress equation we can explicit the component in phase with the deformation and the one not it phase with it

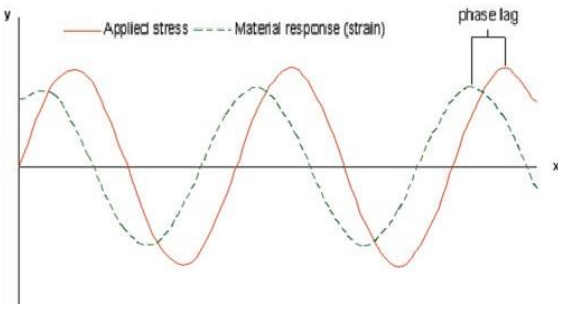

Fig.11: Generic dynamic mechanical analysis of a viscoelastic sample which shows an offset between the input stress and the deformation

$$\tau(t) =$$
$$= (\tau_0 \cos(\delta))\sin(\omega t) + (\tau_0 \operatorname{sen}(\delta))\cos(\omega t)$$
$$= \gamma_0[G'(\omega)\sin(\omega t) + G''(\omega)\cos(\omega t)]$$

where

$$G'(\omega) = {}^{\tau_0}/_{\gamma_0}\cos(\delta) \quad \text{and} \quad G''(\omega) = {}^{\tau_0}/_{\gamma_0}\,\text{sen}(\delta)$$

in which ${}^{\tau_0}/_{\gamma_0}$ is the absolute dynamic modulus, G'(ω) is the storage whereas G''(ω) is the loss modulus. Finally, we can define the complex dynamic modulus G* as the sum of these two moduli, while their ratio is the damping or dissipation factor

$$G^* = G' + iG'' \quad \text{and} \quad \tan(\delta) = {}^{G''}/_{G'}$$

The storage modulus is directly correlated to the energy which is elastically accumulated inside the polymer and that can be released in every cycle, while the loss modulus express the energy dissipated by the viscous behaviour.

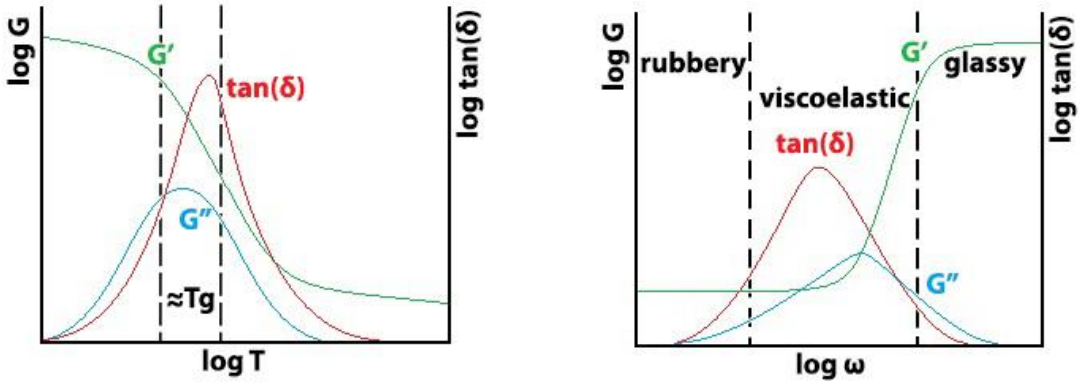

Fig.12: Qualitative variation of storage modulus G', loss modulus G'' and damping factor tan(δ) with temperature and angular frequency. Note that in the first case the peak in energy loss happens at around glass transition, while in the second case we can distinguish three different behaviours.

2.1.4 Hydrogel composition and environment

Mechanical properties, of course, depend strongly on composition since polymers have a wide range of stiffness and hydrophilicity, which are both crucial aspects in a hydrogel. The simplest way to increase the elastic modulus of a sample, if it is not a homopolymer, is to raise the relative amount of physically stronger components or to add a filler with higher mechanical properties; this however will often affect also other aspects of the final

product (for example the hydrophilicity), which in turns can worsen the mechanical properties so it's not always easy to predict the final behaviour [2, 3, 5, 11].

Another easy way to tune the polymer features is to increase the crosslinking degrees, especially because in the swollen state the polymer chains are stretched and spaced with a lot of water in between, so physical entanglements can be too weak. This is achievable both by adding more crosslinking molecules or by higher irradiation doses, if a photopolymerization is performed.

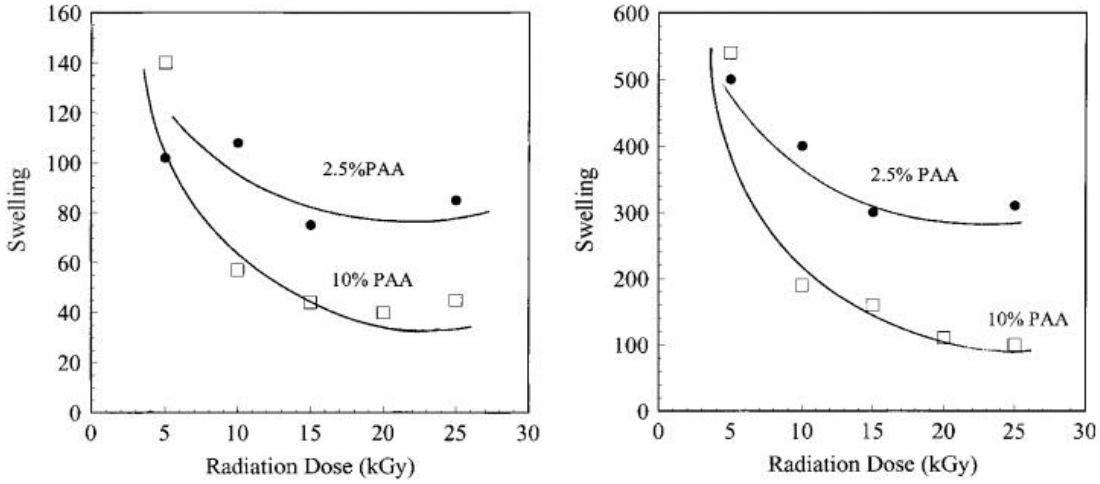

Fig.13: Top: equilibrium weight-swelling ratio $S = (W_{swelled} - W_{dry}) * 100/W_{dry}$ in buffer solution of pH 4 (left) and 7 (right), as a function of γ irradiation dose for 2.5% and 10.0% w/w. A more crosslinked hydrogel has lower chain relaxation potential and less water can be absorbed (which in turn means higher mechanical properties); this is accentuated for more concentrated hydrogel which can form a thicker network of polymeric chains [8].

In the first case, as the amount of active molecules initially increases, the shear modulus of the hydrogel grows in parallel likely due to the increasing number of interchain cross-links; this trend however is not valid for every concentration and in fact we observe a decrease of mechanical properties after a critical value characteristic for the given cross linking agent. This is likely due to the feature of two component hydrogels, as the nature of the cross-linking molecules interferes with the properties of the structural polymer above a certain amount of cross-linking. Note that for what was said earlier the maximum in stiffness is strongly dependent on the type of agent used, however if the concentration is kept below the 5% the resulting shear modulus is unrelated to it [1, 4, 6].

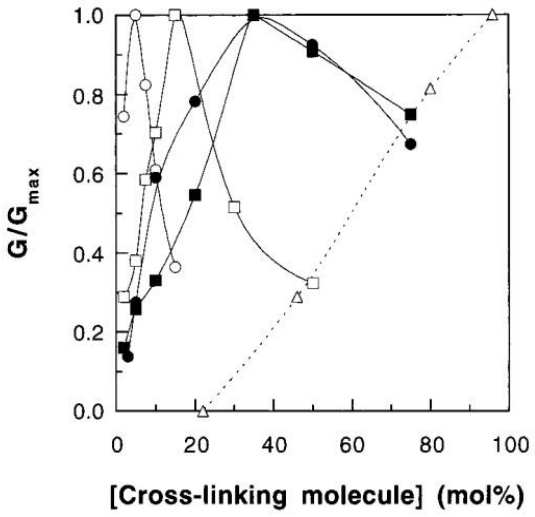

Fig.14: Variation of shear modulus (from compressive test) with the concentration of cross linking agent, for alginate hydrogels with adipic dihydrazide (■), lysine (□) PEGDA1000 (○), PEGDA3400 (●), and Ca^{2+} (Δ) [4].

Once again, when the cross-linking density is altered, changes to properties other than the strength are likely to occur. Diffusivities, and hence release and swelling rates, are likely to be reduced and the maximum degree of swelling is also likely to decrease with a more interchained network [7, 8].

One of the most important aspects for hydrogels is of course the solvent: depending on the type of polymer we are dealing with (whether it forms physical bonds or chemical bonds for example, or the reactivity of its functional groups with definite species and the resulting

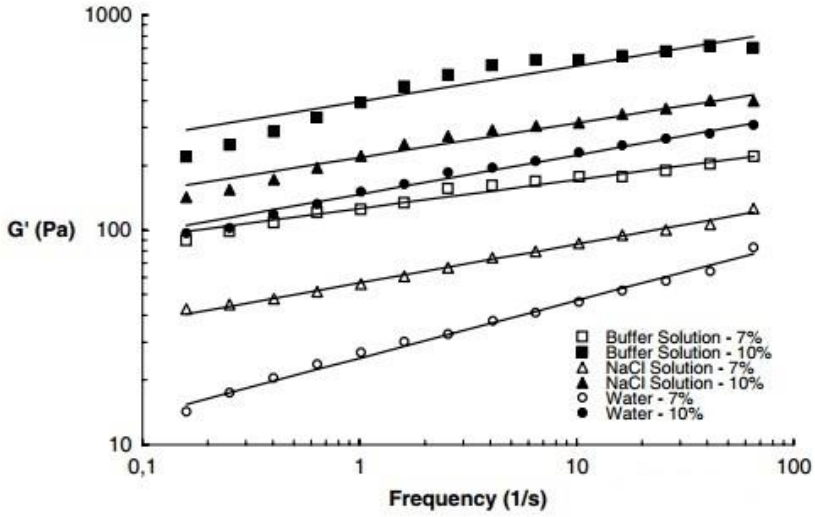

Fig.15: Storage modulus of chitosan–xanthan hydrogel at 7% and 10% concentration in different media. The solution interferes with the normal diffusion and chain relaxation mechanisms, thus altering the mechanical properties and the hydrophilicity of the hydrogel [10].

strength of ionic forces after the polymerisation) the response to parameters such as pH, dilution and solutes varies greatly; a detailed analysis of these properties regarding specific polymers and environments however is beyond the purpose of this thesis, and therefore is left to the papers cited [2, 7, 9, 10].

Nevertheless, a common trend is shared by the majority of hydrogels and that is their behaviour related to dilution during the polymerisation, which is also a main aspect of this study. As we have seen the degree of crosslinking of a polymer is controlled by the fraction of crosslinking agent present in the copolymerization, but it depends also on the double bond conversion that is the percentage of all the crosslinking agent which successfully react to form crosslinks. Potential crosslinking in fact can be lost due to intramolecular cyclization reactions, where both ends of the crosslinking agent bond into the same growing polymer chain, forming a loop structure. Although the equivalent amount of crosslinking agent may be present and incorporated into the network, when cyclization is occurring, the polymer produced is less crosslinked and does not exhibit the expected mechanical properties, equilibrium swelling, and diffusional properties.

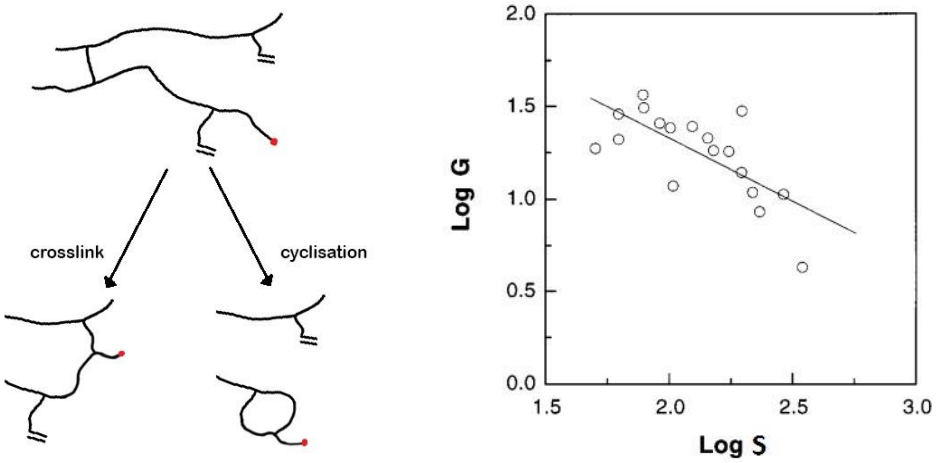

Fig.16: (left) During hydrogel polymerisation the radical (red) can react with double bonds from foreign chains or from its own chain: in the first case crosslinking is achieved, while in the second case we have cyclization [7]. (right) Relation between shear modulus from a compression test and swelling as $S = (W_{swelled} - W_{dry}) * 100/W_{dry}$ [4].

This happens because if the polymerisation is performed with a lot of solvent the rate at which a propagating radical consumes double bonds is reduced thus the active site of the chain will spend more time in proximity of pendant double bonds attached to its own polymer chain. Consequentially it's more likely that it will react with it rather than with a foreign one [1, 7].

These dependencies that we have seen between the mechanical properties and, respectively, copolymer concentration and type, crosslinking, solvent and dilution can be easily transposed to the swelling behaviour of a given hydrogel, since it has been widely documented in fact that stiffness and water absorption are inversely proportional.

First, if our hydrogel is made of two or more polymers, increasing the one with high hydrophilicity or adding a hydrophilic filler will likewise increase the swelling.
A more crosslinked network instead has less room for water, since the chains have a shorter maximum extension and the volume growth will be contained. As we have seen, a higher dilution during polymerisation causes a less crosslinked product, and thus increases the swelling. Once more, the effects of different solutions vary greatly depending on the species taken into account and rely on ionic and network interactions, chemical reactions, etc., but again this fall outside the field of this study and is left to the articles cited [4, 5, 7, 8, 9, 11].

Lastly, mechanical properties obviously change if different reaction conditions for the polymerisation are employed: we can alter reaction time to increase or lower the conversion of double bounds and likewise the temperature or light intensity can be adjusted (for heat- or photopolymerization). Otherwise a post-reaction treatment can be operated (which can be a second heat or light treatment, often applying the one which was not involved in the first reaction, or the addition of compounds that bond with the unreacted specie and tie them to the structure) to prevent the loss of unreacted material and thus increasing the strength of the hydrogel [2].

2.2 Elastic modulus determination

Different methods exist to mechanically characterize a hydrogel and often it is preferred to choose one which is related to the intended application since, as we will see, for this material it is not possible to obtain a single value of, for example, the Young's modulus but the result is strictly contingent to the solicitation undergone.

As we said above, hydrogels show viscoelastic behaviour, so their response to stresses is not linear and is time dependent; to address this problem a series of test can be executed, both with various maximum loads and different deformation rates, to characterize the possible variation in the hydrogel performance. Also, one or more pre-cycle of load and unload may be carried out before the actual measure take place to stabilize the specie behaviour.

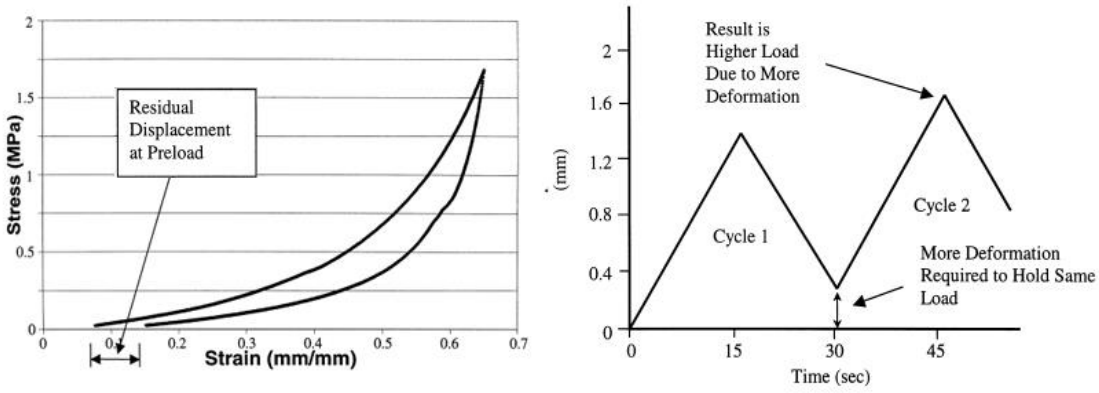

Fig.17: A sample undergoes cycles of load and unload to stabilize its mechanical response before the actual test is performed [12].

A problem may arise while testing, since is generally necessary to characterize the material in its full hydrated status because of the application intended but often the machine performing the experiment does not allow a wet environment. To solve this the specie can be coated in a waterproofing layer which prevents evaporation for the duration of the probing (this is generally petroleum or silicone oil, the second one being more suitable for higher temperature up to 85°C) [1, 12, 15, 18].

2.2.1 Compression

This is one of the simplest test that can be performed to obtain the elastic modulus of a specie; the sample is often cut in a cylindrical shape and placed between two compressing, parallel surfaces to be loaded, while stress and position are recorded and plotted. E can be calculated by fitting the tangent to the graph plotted with σ vs. ε (where σ is the normal

stress and ε the deformation ratio), whereas G is obtained by the Mooney-Rivlin representation

$$\sigma = (C_1 + {C_2}/{\varepsilon})\,(\varepsilon - {1}/{\varepsilon^2})$$

where C_2 has been consistently seen to be approximable to zero, so

$$G = C_1 = \sigma/(\varepsilon - {1}/{\varepsilon^2})$$

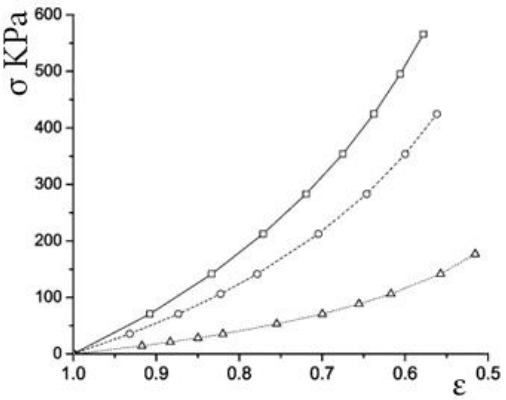

Fig.18: stress-strain curves for compression tests of PEG hydrogels at 10% (Δ), 20% (○) and 30% (□) concentration [14].

For these expressions torsional and horizontal stresses are considered null, which is one of the reasons behind the discrepancies between theory and experimental data at high deformation.

Remember that being hydrogels viscoelastic materials we won't get a constant value of stiffness throughout the test and the mechanical response changes with different shear rates, so which value is to be considered the most satisfactory is related to the final application intended [1, 4, 5, 6, 12, 14, 15].

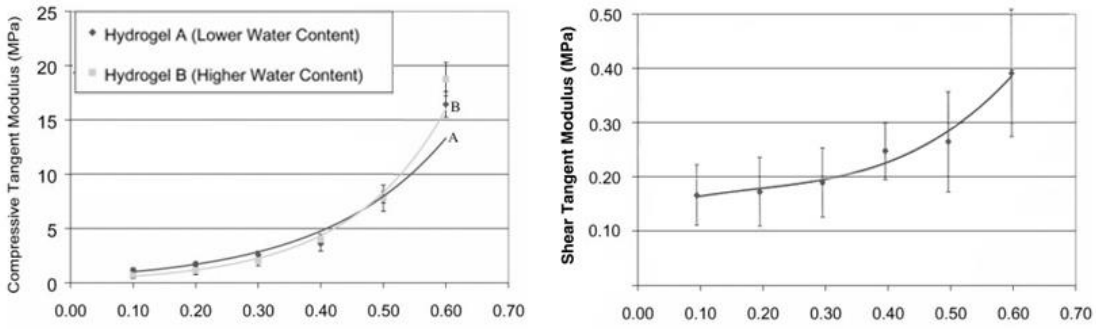

Fig.19: typical trend of E and G for compression test of a lightly crosslinked hydrogel. [12].

2.2.2 Extension

Another common way to characterize a hydrogel is by a tensile test: contrary to what is common procedure with other polymers, the sample doesn't have the typical dumbbell

shape but instead is a cylinder or a parallelepipedon which dimensions are usually around few centimetres in length and circa a centimetre in width, or less. This is due first of all to the difficulty in synthetize a large specimen (which can be expensive or impossible for certain setups, and can lead to inhomogeneities in the final product because of worse control of reaction parameters), and consequentially to complications in making the shape precisely. Lastly, it has been reported that in some cases the grabbing mechanism of the load cell can break more easily the specimen if a width variation is present, thus the preference of the cylinder and parallelepipedon.

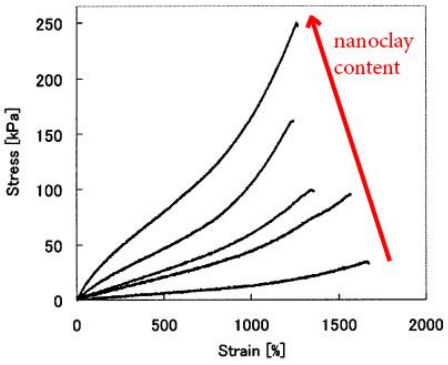

Fig.20: Tensile test on hydrogel with increasing quantity of nanoclay filler[3].

As for before, the response is viscoelastic so we'll see an increase in the Young's modulus with the strain, which is calculated in the same way as for the compression; anyway this method is never used to determine the shear modulus.

An alternative often employed if the hydrogel is at very low concentration or has scarce mechanical properties (so that it's not possible to make a test sample strong enough to endure the standard procedure), is an approximative elongation test: with this analysis a strip of material is fixed on a support and suspended, then a light weight (generally few grams or less) is hanged to its end and the elongation is measured. To obtain the approximate elastic modulus we use

$$E = {}^{P}/_{\Delta L}$$

where P is the weight used and ΔL the stretching of the specimen [3, 16, 17, 20, 21].

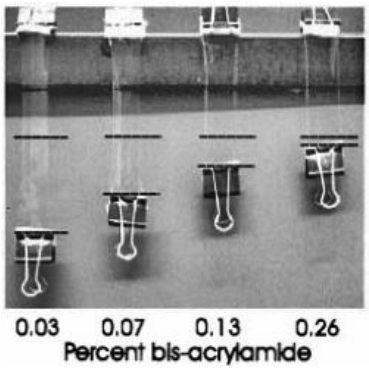

Fig.21: Simplified elongation test, for hydrogels with extremely low stiffness, on an acrylamide sample crosslinked with increasing quantities of bis-acrylamide [3].

2.2.3 Dynamic test

As stated above, since viscoelastic properties depend on the relaxation time of polymeric chains we do expect a connection between the duration of the experiment and the values of mechanical properties found. This can be studied both by varying the strain deformation in a compression/extension test, or with a dynamic analysis: a typical dynamic mechanical tester applies a sinusoidal load in shear mode on one side of the sample while a stress transducer measures the applied stress, on the opposite side of the sample the resulting changes in sample length are measured with a strain transducer.

The sample environmental chamber may be kept isothermal with a sweep of frequencies, or ramped in temperature with a fix frequency. For specific purposes additionally it is also possible to perform a combined test with both a ramp in temperature and frequencies. For a simpler approach and execution, however, the complete viscoelastic behaviour may be determined from several isothermal experiments conducted over a limited frequency range, with the master curve constructed through time-temperature superposition principles.

Aside from the Young's and shear moduli, one important application of dynamo-mechanic analysis is measurement of the glass transition temperature: amorphous and semi-crystalline polymers have different glass transition temperatures, above which the material will have rubbery properties instead of glassy behaviour; moreover with this technique other secondary transitions can be identified, each one associated with different chain sections possible movements, for a complete understanding of the sample behaviour [1, 10, 11, 15, 16, 23].

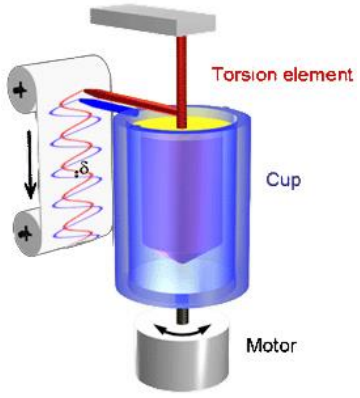

Fig.22: sample instrumentation for dynamo-mechanic analysis.

2.2.4 Macro and micro indentation

In this study, hydrogels were characterized with both these methods, which involve an indenter of specific shape (the most used are a sphere, a paraboloid, a cylinder, a cone or a pyramid) that probes the chosen material while force is registered. The difference between macro and micro is about the dimension of the indenter, that is few millimetres to some centimetres for the first case, and in the scale of the micron for the second one.

Typically for micro indentation there are two different methods commonly used for the measurement of indentation which are called the imaging method and compliance method. In the imaging method, the indenter penetrates in the sample surface with a specific load and retracts after a specific dwelling or residence time. The diameter or diagonal of the residual image of the indentation trace is then measured by optical or other methods. However, this method has some inherent limitations. The imaging of the residual indent becomes inexact as the indentation size is scaled down, and moreover, considerable viscoelastic recovery with time of the residual imprint can take place. Therefore, this method provides primarily the plastic response of the material, or the viscoelastic-plastic properties of organic polymers, which creep in the indentation region significantly after unloading.

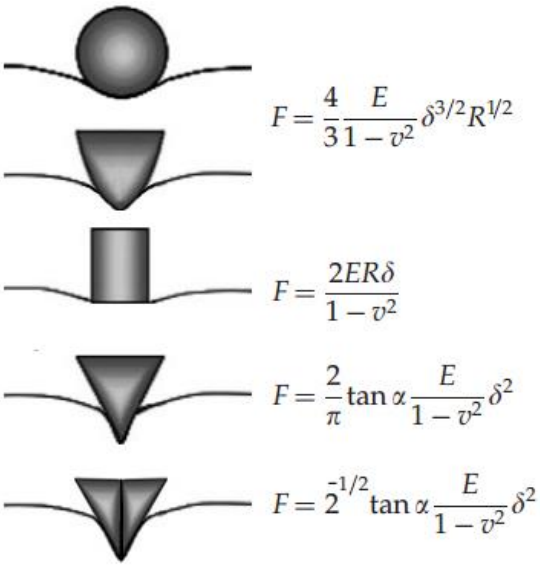

Fig.23: elastic response according to Hertzian model for different indenter geometries: sphere, paraboloid, cylinder, cone and pyramid. Note that spherical and parabolic probes share the same equation [25, 26].

The surface mechanical properties such as stiffness, hardness, and elastic modulus are obtained both in the micro and in the macro indentation from the analysis of the force-displacement data recorded during loading-unloading indentation cycles performed upon material surfaces: this is as said before the compliance method. To obtain the elastic behaviour of the material studied from the experimental data different theoretical approach

can be chosen, however the Young's modulus is generally evaluated from a formula which is typical for the shape of the indenter, that links the force F and the indentation δ through the Poisson's coefficient ν and geometric constants of the indenter (which are the curvature radius R or a specific angle α, see bibliography for more details).

These formulae come from the Hertzian method that idealizes the sample as an isotropic, linear elastic solid, so it can be assumed that there is no other interaction more than elasticity and therefore no plastic deformation between the sample and the tip.

This of course is hardly true at low concentration or for lightly crosslinked hydrogels, especially for the micro indentation where adhesives phenomena become evident, so different values of Young's modulus are found depending on the setup employed. [24, 25, 26, 27, 28, 29, 30, 31]

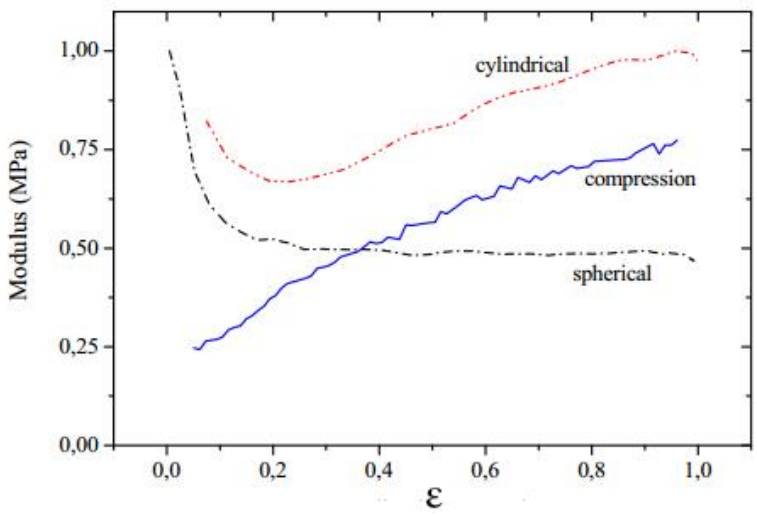

Fig.24: Young's modulus variance with different evaluation methods (indentation and compression test) and different indenter geometries (cylindrical and spherical) [24].

Also, it is important to note that generally the Poisson's coefficient is approximated as ν = 0,5: this is reasonably true for relatively fast macro indentation because, when a load is suddenly applied to a hydrogel, water molecules don't have enough time to migrate into or out of the polymer network right away; consequently, the volume of the hydrogel is conserved and the instantaneous value of Poisson's ratio is very close to 0.5. This is not actually correct in the micro scale where the distances of water migration are reduced and the network is more capable of accommodating these small fluctuations in water content. As a result we can have a variation in the range of 0,7-0,3 [13, 25, 31]

2.3 Stiffness effect on living cells

The importance in studying the mechanical properties of hydrogel relies on their employment as a substitute for mimicking biological environments: for years cells have been cultured in polystyrene or glass petri dishes with planar geometry, but more recently there have been a drive in replicate as much as possible the in vivo conditions that should normally surround a living cell; this include both the geometrical aspect and the mechanical response that normally associate with the source biological tissue.

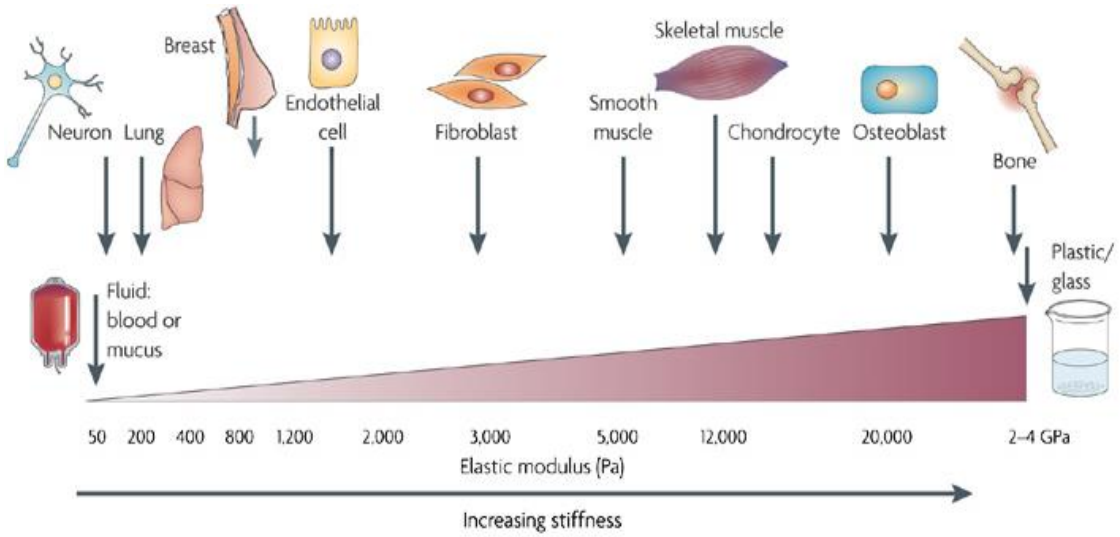

Fig.25: Stiffness ranges for different biological tissues.

As a general rule, stiffness and strength of a tissue should be in relation to the physical solicitation undergone by said tissue; low stresses in brain and fat may explain why these tissues are soft, while high stresses on adult bone are thought to promote its growth and stiffening through a "mechanostat" that functions to match the stress. At a microscale, physical stress deforms cells and alter gene expression profiles; cells in vivo directly sense the local tissue stiffness or microelasticity and react accordingly: several studies have found that gels that mimic the compliance of brain or fat, respectively, maximize neurogenesis or adipogenesis, gels that are moderately stiff like muscle are best for myogenesis, and gels that are firm like precalcified bone optimize osteogenesis in 2D and 3D. This happens because by mechanotransduction systems, cells adhere to the extra cellular matrix, pull it and translate these reaction stimuli into biochemical signals controlling multiple aspects of cell behaviour, including growth, differentiation and cancer malignant progression; the

result is a stiffness-driven change in morphology and cell specification which affect not only healthy cells, but most interestingly the development and evolution of cancerous one [32, 33, 34, 35].

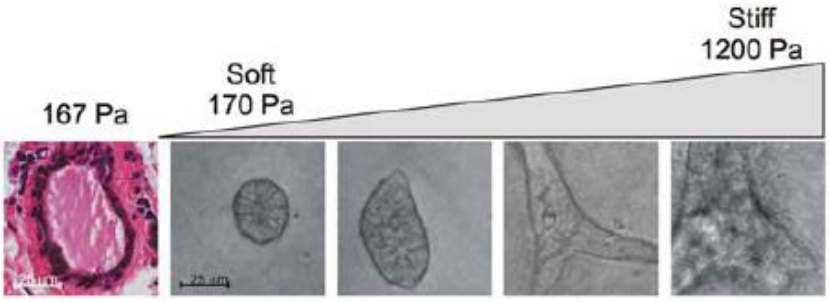

Fig.26: typical morphology of a mammary gland duct in a compliant gland (167 Pa), compared with colonies grown in gels of increasing stiffness [34].

For this reason, finding a way to recreate different biological environments with high accuracy is a key aspect in the future of medical research, and to do so we have to comprehend how materials behave at a micro-scale and how to reproduce them.

Chapter 3

Materials and methods

3.1 Hydrogels synthesis

For this study two different hydrogels were employed, which are poliethylenglycoldiacrylate Mn = 700, and an acrylamide/bis-acrylamide 29:1 mix at 40% w/w concentration, both from Sigma Aldrich; this choice was made because they are between the most commonly used polymers for biological and other applications, so results are easily compared with literature.

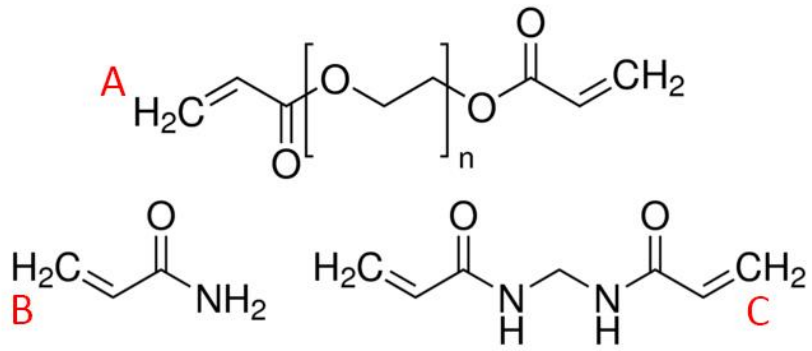

Fig.26: A) polyethilenglycoldiacrylate, B) acrylamide, C)bis-acrylamide.

A thermal polymerisation was preferred because for the replica moulding the silicon master was employed instead of a PDMS replica, and due to the high aspect ratio of the pillars a good UV irradiation was not achievable. Two different initiators had to be used since for PEGDA stability issues were observed

3.1.1 Solution preparation

Both PEGDA and PAA underwent the same protocol to obtain the desired solution at a given concentration ready to polymerize, and that is:

Polymer	Polyethylenglygoldiacrylate Mn 700	Acrylamide/bis-acrylamide 29:1, 40%
Initiator	WAKO VA086	WAKO VA057
Fluorescent agent	Rhodamine 6G	

Tab.1: Chemicals employed for hydrogel polymerisation.

1. The desired amount of polymer is taken from the refrigerated stocking and poured in a glass vial, then it is let to heat at room temperature to lower gas solubility.
2. The vial is kept in an exicator under vacuum for 10 minutes, after which nitrogen is fluxed in to create an inert atmosphere.
3. In said exicator a tube tipped with a cut Pasteur pipette is introduced and nitrogen is bubbled through the polymer for 2 minutes. This will strip any oxygen left from the vacuuming step.
4. The vial is removed from the exicator, keeping a high flux of nitrogen to its opening during the process to minimise oxygen contamination, and closed.
5. A second vial is prepared, containing the required amount of distilled water for the final desired hydrogel concentration, and the thermal initiator which is 2% of the total polymer weight.
6. Step 2 and 3 are repeated for this solution. Keeping the polymer and initiator separated is a crucial aspect of the protocol: performing the nitrogen bubbling after the two are mixed may cause an unwanted polymerisation, the cause of which is not clear.
7. The water and initiator are poured in the polymer vial, again under nitrogen flux, to obtain a slightly turbid solution. After few seconds of agitation a clear, homogeneous mix is obtained.
8. The liquid is either polymerised right away or it is sealed with parafilm and stocked refrigerated.

This procedure was proven to guarantee a sufficient low concentration of oxygen which would interfere with the polymerisation, bonding with the free radical of the initiator; particularly at low concentration there can be a complete inhibition of the reaction with no gel formation whatsoever.

It is interesting to notice that PEGDA is more susceptible than PAA to this phenomenon, reason why the first polymer was employed to test the mechanical properties at high

concentration (from 60% to 10% [polymer weight/total solution weight %]), while the second one was studied for higher water content (from 20% to 5% [polymer weight/total solution weight %]).

Rhodamine was added as a fluorescent agent just in the samples that had to be analysed by the confocal microscope: an arbitrary small quantity (roughly a milligrams per 5 grams of solution) was added during the mixing process, enough to colour the solution of a bright red.

3.1.2 Bulk polymerization

For what we just said, the inert atmosphere had to be maintained throughout all the process: this was achieved with the employment of a glass container with a rubber seal and a mechanical closure. To ensure minimum contamination from oxygen the following procedure was performed:

1. The glass container is placed, open, in a large exicator with a petri dish (3,5 cm in diameter) inside it.
2. The hydrogel solution is poured from its vial to almost fill the petri (little room is left to account for volume increase due to swelling after polymerisation is completed).
3. Rapidly, the glass container is partially shut (enough opening is left for air to flow out and nitrogen to go in afterwards) and the exicator is closed. Vacuum is applied for 10 minutes.
4. Nitrogen is fluxed in, then the exicator is opened and quickly the glass container is sealed by its mechanical closure.
5. Polymerisation is carried out in the oven at 75°C

Fig.27: Sealed glass container employed in bulk polymerisation to keep the inert atmosphere.

The duration of the heat treatment depends on the hydrogel concentration: an increasing water content lowers the chance of two chains to reach one another as stated in the previous

chapter, so higher dilution calls for longer stay in the hoven to ensure that all the monomer has reacted.

Polymer	$\frac{\textbf{Polymer weight}}{\textbf{Total solution weight}}\%$	**Time [min]**
PEGDA	60%	120
	30%	120
	20%	150
	10%	180
PAA	20%	40
	10%	60
	7%	90
	5%	90

Tab.2: Heat treatment duration for different hydrogel concentration.

Nonetheless, in PEGDA based hydrogels polymerisation issues were observed: both 20% and more evidently 10% showed a layer of unreacted liquid (a thin film for the first one and ca. a millimetre for the second) on top of the petri dish, and a slightly irregular, wave-like surface. Prolonging the heat treatment did not affected the outcome of the synthesis so this is very likely due to traces of oxygen present in the sealed glass container during the process.

3.1.2.1 Samples for swelling

To measure the swelling properties of our hydrogels specific paralepidid specimen were produced; the procedure is the identical to the bulk polymerisation, but a custom die is placed inside the glass container instead of a petri dish.

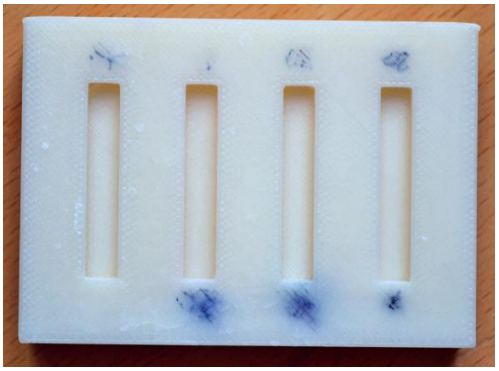

Fig.28: Die employed for swelling samples polymerisation.

3.1.2.2 Washing and swelling

Samples were removed from their petri dishes and let to soak in distilled water, this had two purposes: first of all the unreacted monomer is extracted from the bulk, and to achieve

this water was changed every day for 4 days; secondly, hydrogels can swell and reach their equilibrium water concentration, which causes volume to increase.
Once completely swelled, excess material was cut to get the specimens to fit again in the 3,5 cm petri dishes, then they were kept under a mix of distilled water with the addition ≈5% pure white alcohol, to prevent the formation of microorganisms.

3.1.3 Pillars replica moulding

3.1.3.1 Functionalisation

Chromium remover	Hydrochloric acid 40%
Piranha etch	Sulfuric acid/Hydrogen peroxide
Silicon master functionalisation	Octadecyltrichlorosilane (ODTS)
Solvents	Heptane/Acetone

Tab.3: Chemicals employed for silicon master functionalisation.

The replica moulding process is about casting a micrometrical design by pouring the hydrogel over a structured surface, polymerise it over a glass slide and then release it to retrieve the final pillar array.
As mould a silicon master was employed: this was obtained with a chromium mask on a silicon wafer and pillars have been plasma etched on it. Before any treatment can be done we must first remove the chromium which passivates the surface, and that is achieved by dipping the master in hydrochloric acid for ten seconds followed by washing with distilled water.
The piece is now ready for the silanization which is carried out as follow:

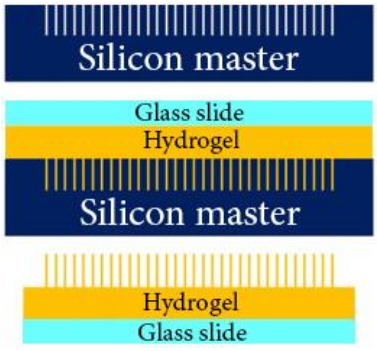

Fig.29: Schematics of replica moulding process.

1. A piranha solution is prepared by slowly pouring hydrogen peroxide into sulfuric acid with a ratio of 3:7 respectively; the mix is placed on a heater at 100°C.
2. The silicon master is etched for 20 minutes, shacked approximately every 5 minutes to remove bubbles from its surface and prevent floating.

3. After washing the piece in distilled water it is let to completely dry on the heater at 100° for 10 minutes.
4. A functionalising solution (197 μL of ODTS for every 100 mL of heptane) is prepared, this must be done in a glovebox filled with argon due to the high sensitivity of the ODTS to water and humidity.
5. The master is let 30 minutes to silanize before being cleaned: then it is extracted from the glovebox in a falcon filled with heptane, stirred to clean off the excess ODTS and finally washed first with acetone and successively with distilled water. These two steps must be done rapidly enough not to let the solvent film evaporate, in fact if part of the surface dries before being washed with water a halo will appear, which will cause worse pillars replica.
6. The master is dried with compressed air and is ready to use.

This procedure is performed to facilitate the release and to avoid that residues remain inside the holes. However, after 2-3 uses the silanization wears off and some hydrogel get stuck in the silicon wells: this calls for a cleaning cycle that consist of a first phase in the hoven for 3 hours at 270°, and a second phase which is a piranha etching as described above for about an hour. After this the master is ready for step 3 of the silanization.

Glass slide functionalisation	Trimethoxysilylpropylmethacrylate (TMSPM)
Solvents	Acetic acid/Ethanol

Tab.4: Chemicals employed for glass slides functionalisation.

A said, the hydrogel is polymerised over a glass slide which will support it after the peel off, but to obtain a good adhesion between the two the base has to be functionalised too:

1. First of all glass slides are cleaned with soap and dried with compressed air not to let some paper traces on its surface.
2. The functionalising solution is prepared adding 50 μL of TMSPM to 1 mL of ethanol and acetic acid solution (950 μL of the first and 50 μL of the second).
3. Slides are plasma treated for 2 minutes and covered with the functionalising solution for 5 minutes.
4. They are washed in pure ethanol and, still wet, let in the hoven at 100°C for 10 minutes.

TMSPM has one end of the chain that bonds with the glass, while the other acrylic end will react with the hydrogel securing it to the surface.

3.1.3.2 Replica moulding

Now that both the silicon master and glass slides are functionalised, we can proceed with the pillar synthesis: two methods were tested for the reproduction of the microstructure, the first more simple one is the "droplet setup" and the more complex is the "pool setup", which are described below.
Note that for this synthesis there is no need to keep an inert atmosphere because the glass slide seals the pillars area, so even if oxygen diffusion is observed, the phenomenon is localised to the edges of the slides (where the hydrogel remains liquid) and is not a problem.

Droplet setup

1. The silicon master in placed in a petri inside an exicator and hydrogel solution is poured over it with a Pasteur pipette, enough to cover the etched pillars pattern.
2. Vacuum is applied for 10 minutes to empty the master from air; bubbles will appear and coalesce escaping the droplet (tapping the exicator will aid this process).
3. Nitrogen id fluxed in and rapidly a glass slide is pressed onto the master: excess solution will form a "protective" ring from oxygen around the edge of the sample.
4. The hydrogel is polymerised at 75°C (look at table 2 for duration) and taken

Pool setup

1. The silicon master is placed on a sloped plane over a pool of hydrogel solution, inside an exicator.
2. Vacuum is applied for 10 minutes
3. Tilting and tapping lightly the exicator the master is slid inside the pool
4. Nitrogen is fluxed in then, keeping the sample under nitrogen flux, the master is removed and placed on a petri; some solution is collected from the pool with a Pasteur pipette and poured on the etched area.
5. A glass slide is pressed onto it, forming a "protective" ring of excess solution, as per the droplet setup.
6. The hydrogel is polymerised at 75°C (look at table 2 for duration) and taken

out of the oven to cool for a minute, after which pillars are released.

out of the oven to cool for a minute, after which pillars are released.

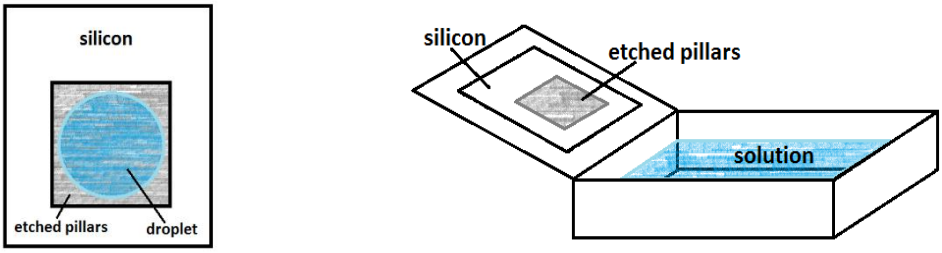

Fig.30: Droplet setup (left) and pool setup (right) for pillars replica moulding.

3.1.3.3 Washing and swelling

Analogously to the bulk samples, pillars were let in abundant distilled water to extract the unreacted material and swell, however since dimensions are much smaller and surface area is way greater than the previous case, we can assume that complete diffusion occurs in much less time. Water is therefore changed just one time and after a day before starting the characterisation.

3.2 Hydrogel characterisation

3.2.1 Macro indentation

In this study indentation was performed with a sphere of 60 mm diameter, three different measures were performed on the same sample with two indenter speeds (0,1 mm/s and 1 mm/s) with no noticeable difference in the final elastic modulus, so final tests were performed at the higher one.

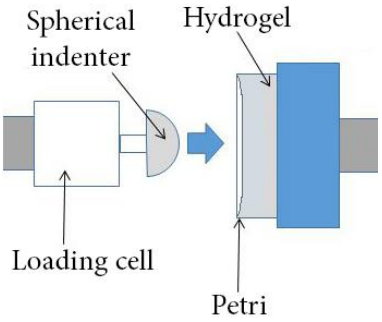

Fig.31: Indentor schematics .

To analyse experimental data the Hertzian method was adopted: according to this theory the sample is an isotropic, linear elastic solid, so it can be assumed that there is no other interaction more than elasticity and therefore no plastic deformation between the sample and the tip. For the macro indentation the evaluation of Young's modulus was done following the assumption of the material behaving like a Mooney-Rivlin hyperelastic incompressible model defined by the function of deformation energy

$$W = C_1(I_1 - 3) + C_2(I_2 - 3) + p(\sqrt{I_3} - 1)$$

Where I_1, I_2, I_3 are the invariants of the deformation tensor of Cauchy and p is hydrostatic pressure, while C_1 and C_2 are obtained by experimental data. Considering the Hertzian contact problem, the analytic solution gives us the reaction force as a function of indentation, which for the considered model is

$$F = B_1\pi\left(\frac{a^5-15Ra^4+75R^2a^3}{5Ra^2-50R^2a+125R^3}\right) + B_2\pi\left(\frac{a^5-15Ra^4+75R^2a^3}{-a^3+15Ra^2-75R^2a+125R^3}\right)$$

Where $a = \sqrt{R/\delta}$, being R the radius of the indenting sphere and δ the indentation depth. B_1 and B_2 are parameters linked to previous invariants, they are obtained via minimisation of the error between experimental data and theoretical behaviour, while the initial tangential elastic modulus E_0 is calculated as

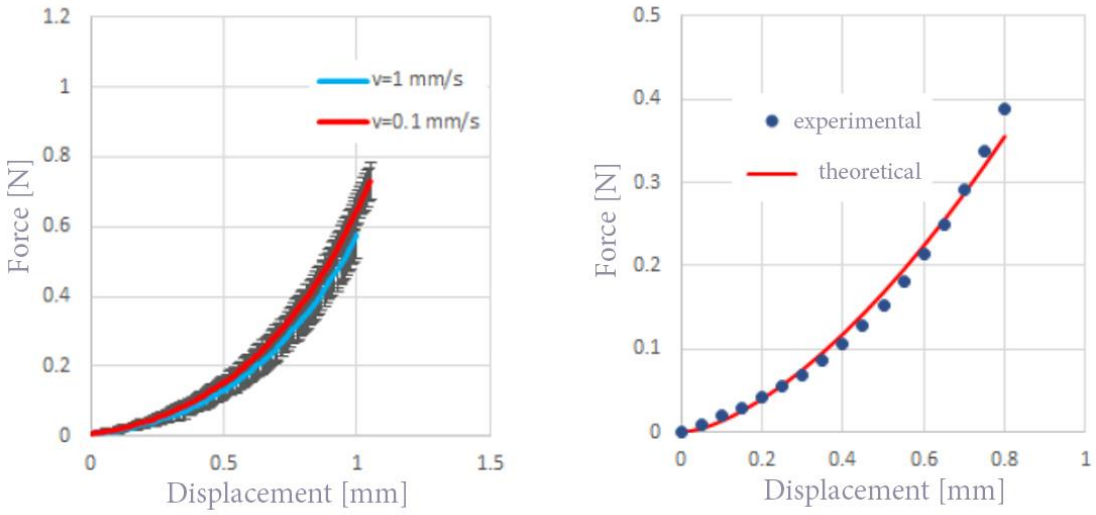

Fig.32: on the left, sample experimental curves at two different indentation speeds for the same hydrogel; no substantial differences were observed in the final result. On the right, comparison between experimental data and theoretical fitting.

$$E_0 = (B_1 + B_2)\,(1 - \nu^2)\,{}^{9\pi}/_{20}$$

Since we are using an incompressible model, Poisson's coefficient is set as 0,5; experimental data are calculated up to indentation of 0,8 mm so that the mechanical response will be almost elastic, and the Mooney-Rivlin model can be employed. Moreover, due to the small indentation depth relative to the total high of the sample we can consider the analysis to be done on an semi-infinite plane so that there is no influence on the elastic modulus value calculated.

Previous equations are valid only under the condition $a/R < 0.4$, but

$$a = \sqrt{R\delta} = \sqrt{30 * 0.8} = 4.9$$
$$a/R = 0.163$$

so this theoretical treatise is correct.

3.2.2 AFM micro indentation

Young modulus has been tested at microscale by using a Park Instruments XE-Bio AFM through the distance-force measurement: the curve is obtained by measuring the tip-sample

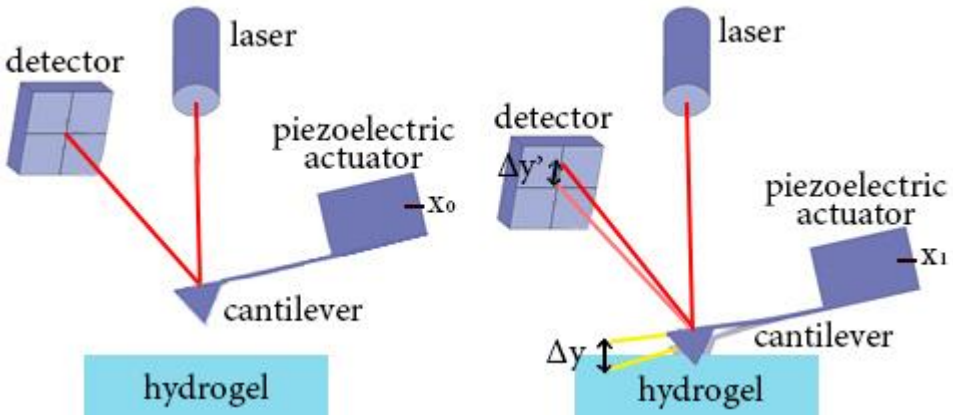

Fig.33: Schematics of AFM functioning: the piezoelectric actuator gives the relative position of the cantilever tip while a laser tracks the cantilever bending; when unsolicited the laser is reflected at the centre of the photodiode, it moves when the cantilever is loaded of a quantity Δy' from which Δy is calculated and the force is obtained by the spring equation $F = k * \Delta y$, where k is the spring constant.

interaction force along with the vertical displacement of the cantilever during the push-in/retraction process. The tip-sample force is derived by using the measurement of the cantilever deflection and the knowledge of the effective spring constant of the cantilever which behaves like a spring since only elastic deformation occurs.

3.2.2.1 Preliminary measures

At first, AFM was used with default settings which means that the curve given by the software is set to force-distance: in this mode, the instrument treats the cantilever as infinitely rigid and ascribes all vertical displacement to sample indentation. This however is far from the actual behaviour of the indenter: when the tip enters in contact with the sample, the cantilever will deflect to the opposite direction; hence, in addition to indentation depth, cantilever bending must be considered which is proportional to F/k (with k=cantilever spring constant). The significant parameter is called sensitivity and is calibrated at the beginning of the measure session by probing a hard substrate such as silicon: since we can assume that no indentation occurs, all the displacement registered is ascribed to cantilever bending and will be subtracted from subsequent measures.
The revised plot of the cantilever deflection in XEI will transform to display a force-separation curve and this will be used for calculating the value for E.

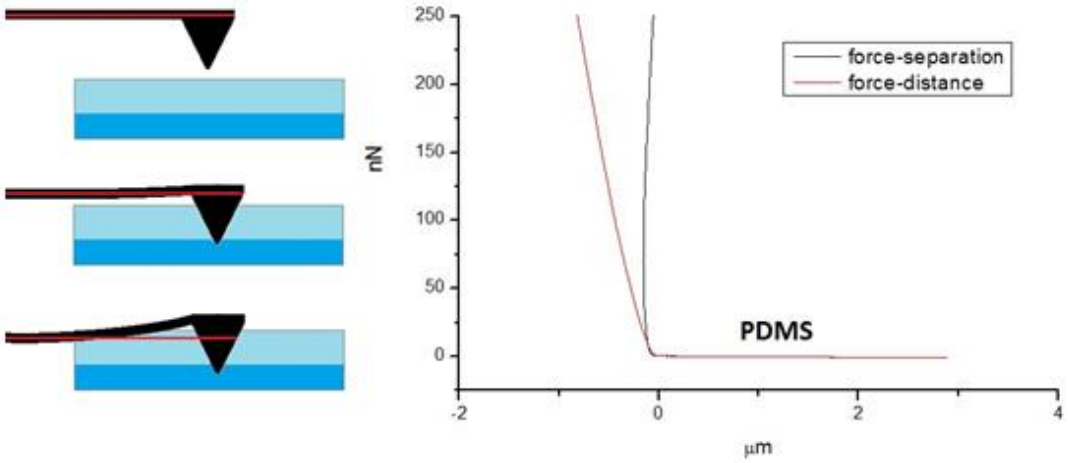

Fig.34: On the left, increasing cantilever bending with deeper indentation; on the right, force-separation and force-distance different curves for the same PDMS sample.

Another important parameter is indentation depth: initially we decided to probe our sample up to 12-13 µm to have a clear and complete curve from which extrapolate mechanical data,

however this is not the right approach when interpolating with the Hertzian model: we already said that according to this theory the sample is an isotropic, linear elastic solid, and that can be considered true for small, reversible deformations. Nevertheless, with higher indentation depth we irremediably enter the field of irreversible, plastic, nonlinear deformations, and it can be seen from the graph below that the theoretical exponential curve of the Hertzian model stop fitting well experimental data over a certain depth.

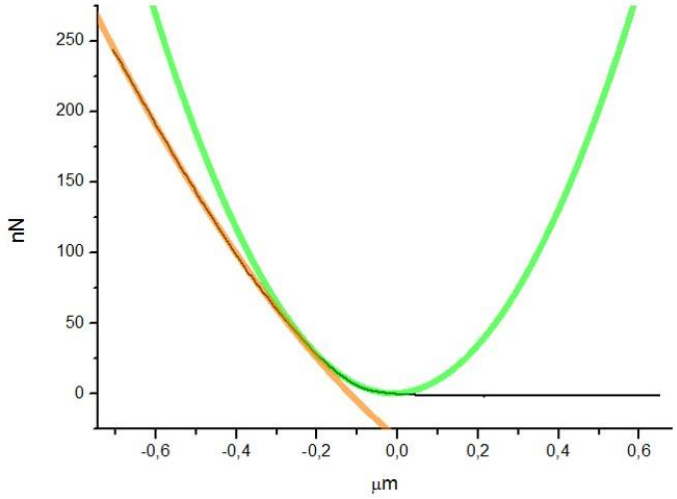

Fig.35: Experimental curve with two Hertzian model fitting: we can clearly see two different regions with different mechanical response, much likely in the macroscale we have a first linear response and a second nonlinear behaviour. It is not possible to have a single fitting with reasonably low error.

3.2.2.2 Final measures

After this preliminary setup, the elastic modulus is calculated from plots of the tip-sample interaction force vs. the indentation depth through the AFM software, which employs the Hertzian model as described above: it will calculate Young's modulus E in function of force and indentation and its parameters depends on the indenter tip geometry; for the pyramid we have

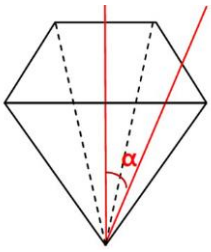

Fig.36: Indenter tip geometry.

$$F = \sqrt{2}\ \tan(\alpha)\ \frac{E}{1-\nu^2}\delta^2$$

where F is the force, α is the angle shown in the picture above, ν is the Poisson's coefficient, δ is the indentation.

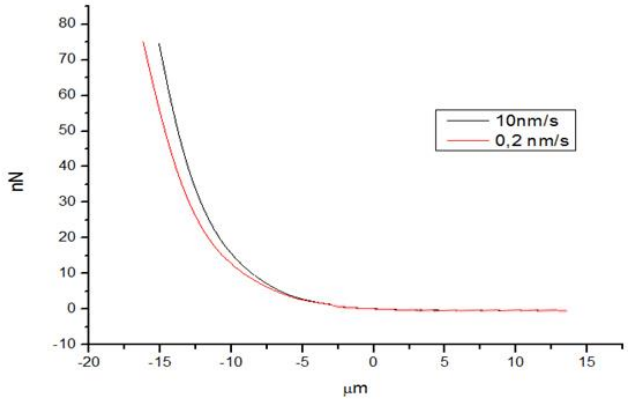

Fig.37: PAA 7% at two indentation speeds: the difference in the elastic response becomes visible only at high indentation depth, in the 2-3 μm zone hydrogel behaves almost the same.

Tests were done at 0,2 μm/s speed with an indentation depth of 2-3 μm (depending on the response of the single sample), as for the macro indentation the effect of indentation speed was tested with a measurement done at the maximum and minimum speeds possible with this instrument: hydrogel turned out to behave slightly stiffer with higher speed, however the slowest setting was preferred since the modulus increase is small and to keep the results comparable with literature.

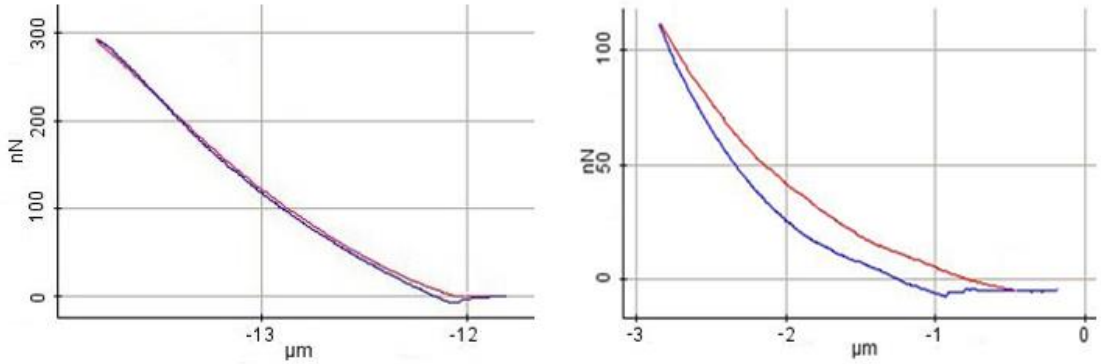

Fig.38: Sample curves of AFM indentation for PEGDA 60% (left) and PAA 10% (right). The adhesive effect is greater and clearly visible at low concentration, while for high concentration is delimited to the very end of the unloading curve.

Only the loading curve was used to calculate the Young's modulus: this is because in the unloading phase the force is typically lower due to adhesive phenomena; in fact when the tip retracts, especially approaching the beginning of the curve, hydrogel is glued to the indenter and pulls it downward so that the upward force that normally resists the penetration seems lower.

Even with small indentation depth we still have irreversible plastic deformation, especially for softer substrates.Nevertheless since we cannot quantify the magnitude the phenomenon it won't be taken into account. For stiff samples this is not an excessive approximation, however it becomes more and more evident the softer the hydrogel, to the point that for PAA at 5% and 7% curves are quite noisy and often no useful data can be obtained so the test has to be done again.

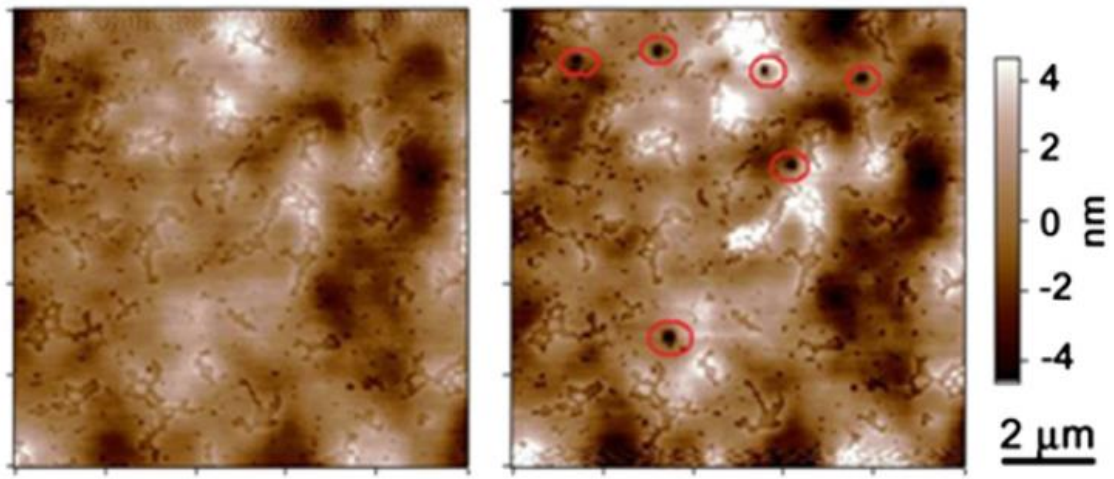

Fig.39: Topography of hydrogel surface before and after the test, indentation marks are visible implying an irreversible deformation of the sample which is at the base of the difference between analytical and experimental data [36].

Since the values obtained from AFM are sensible to the positioning of the cantilever and the setting of the instrument, to verify the accuracy of the results a reference PAA sample (prepared as described in literature [41]) was measured every session before testing anything else; if the found value was not equal to that given in literature the cantilever was replaced and settings was done anew.

All measures were done with the hydrogel being submersed in distilled water to prevent evaporation during the test and thus incorrect moduli values. For each sample at least 10 measures were done, each distant at least 25 μm from the others, however PAA at 5%, 7% and 10% were tested up to 30 times since the elastic modulus seemed to be oscillating more widely around a mean value unlike hard samples which have lower standard deviation.

3.2.3 Compression and stress relaxation

Hydrogel were also tested in compression in order to have a set of data obtained in a classic way, comparable with values found in literature. An Instrong 1121 extensometer was used which clamps, intended for extensions tests, were adapted for a compression test adding

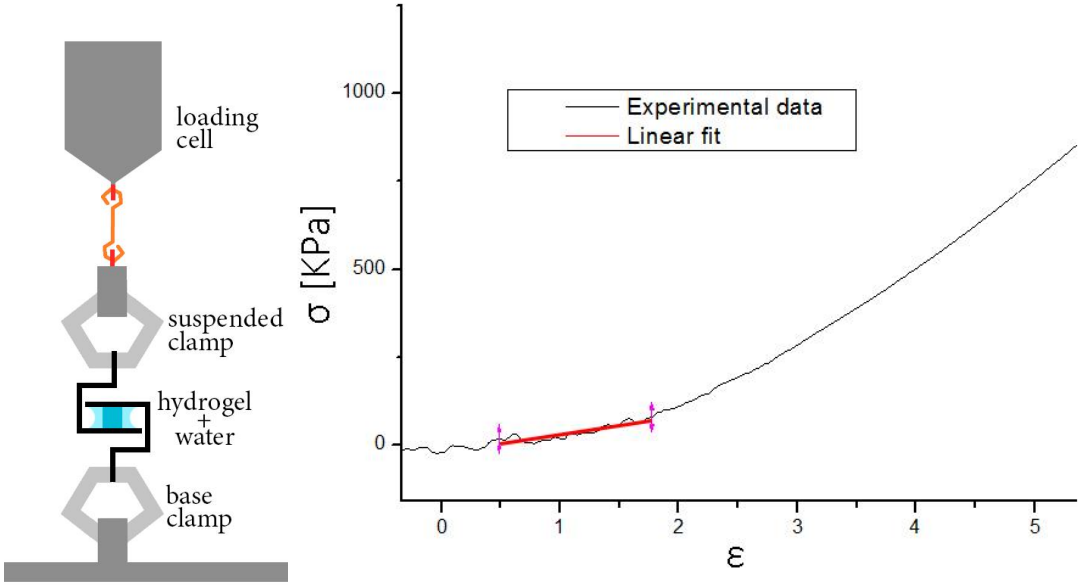

Fig.40: On the left, schematics of compression test, on the right a sample compression curve and interpolation of the first linear region; from the graph we can identify a first noisy "settling" region, and a second more clear high stress region.

two metal sheets as in figure 30; a piece of sand paper was glued to both metal sheets to prevent hydrogel from slipping and water was added to completely cover the sample to prevent evaporation, as for the AFM. For this test the petri dishes used up to now were too large to fit in the instrumentation, so smaller cylinders were obtained from them using a puncher of diameter 20,5 mm.

With this instrument compression speed was restricted to a number of pre-set values, so 50 mm/min was selected because it was the closest to that employed in the macro indentation; compression was performed three times and elastic modulus was calculated through interpolation of the first linear section of the curve. As we see in the image below, the first low stress region is characterised by high noise compared to the high stress region: this is probably due to the fact that the suspended clamp is hanged to the loading cell and can swing freely, so when the hydrogel, placed on the top metal sheet that moves upward, comes in contact with the other metal sheet, which is fixed to the base, there are tiny settling movements that perturbate the measure.

To calculate hydrogels' diffusion constant a relaxation measurement has been performed: as suggested in literature [37] an even smaller cylinder was cut from the initial hydrogel, because water will migrate from the inside to the side surface of the sample so to a smaller radius correspond a lower relaxation time which is more easily measured. All hydrogels were compressed ≈2 mm and data were collected for 30 min: even if some of the softer were completely relaxed after this period, most samples did not achieve their steady state (we calculated that for PEGDA 60% it would take almost 4 hours) so we proceeded with a theoretical prediction of their behaviour. We can see from the curve in fact that after a fast stress decrease that occurs in the first couples minutes samples keep on relaxing following an exponential trend; we fitted the second part of the curve with almost no error to obtain the total relaxation time, which was calculated as the point at which the difference between the exponential curve and its horizontal asymptote was 0,01% of said asymptote, that is

$$(Y - Y_0)/_{Y_0} = 0.01\%\, Y_0$$

which gives

$$X_{relax} = (-t)\, log\left(0.0001 * Y_o/_A\right)$$

Where Y, Y_0, t and A are parameters from the exponential fitting shown below.

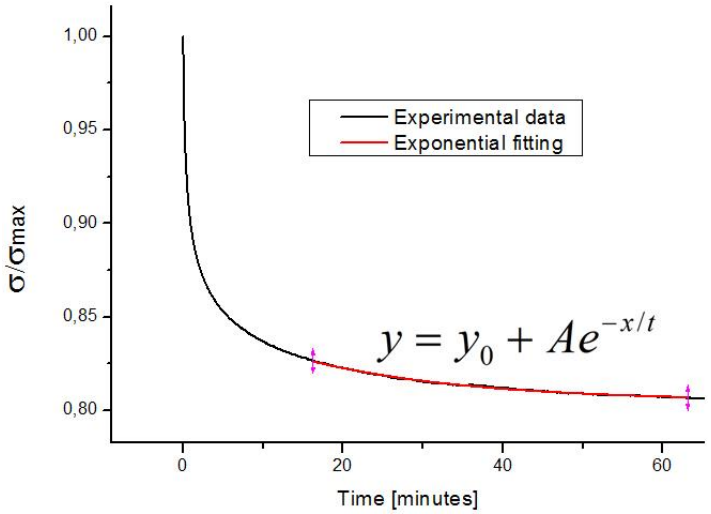

Fig.41: Sample experimental curve of a PEGDA 60%, characterized by a first rapid decrease in stress and a second exponential decrease. The last one can be fitted to extrapolate the hydrogel behaviour for longer time and calculate the relaxation time.

This procedure was chosen to minimize the error from arbitrary choosing the relaxation time for every curve; also, it has been checked that even for low concentration hydrogels, which had fairly great variance of fitting results (based on which interval of data was chosen for the interpolation), the final diffusion constant value was almost identical, since all fitting converged to the same curve at longer time. Even the threshold value of 0,01% had small relevance on the final data, and similar results can be obtained for percentages up to 1%

.

Chapter 4

Experimental results

4.1 Swelling

This was the first, most simple but important hydrogel characterisation since swelled samples were produced alongside with the bulks; we see that, as expected, at higher polymer concentration corresponds lower swelling and as we will show, higher mechanical properties, as said in the state of the art. Swelling was calculated as

$$S_W\ \% = \frac{W_{swell} - W_{dry}}{W_{swell}} * 100$$

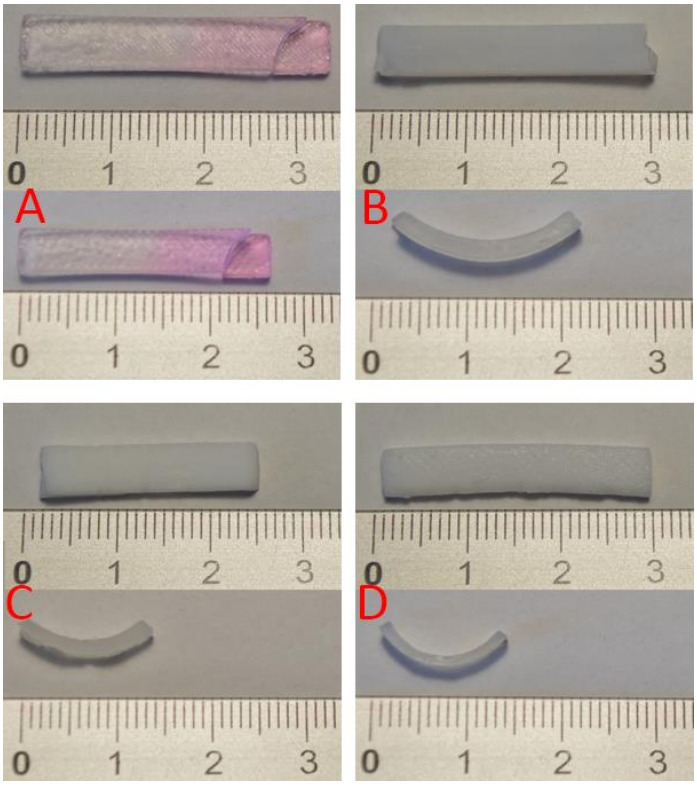

Fig.42: PEGDA samples at swelling equilibrium and completely dry. Their concentrations are A) 60%, B) 30%, C)20%, D)10%.

Where W_{swell} is the weight of the sample at swelling equilibrium and W_{dry} is the sample after 3 days in air and one day in a sealed exicator under vacuum.

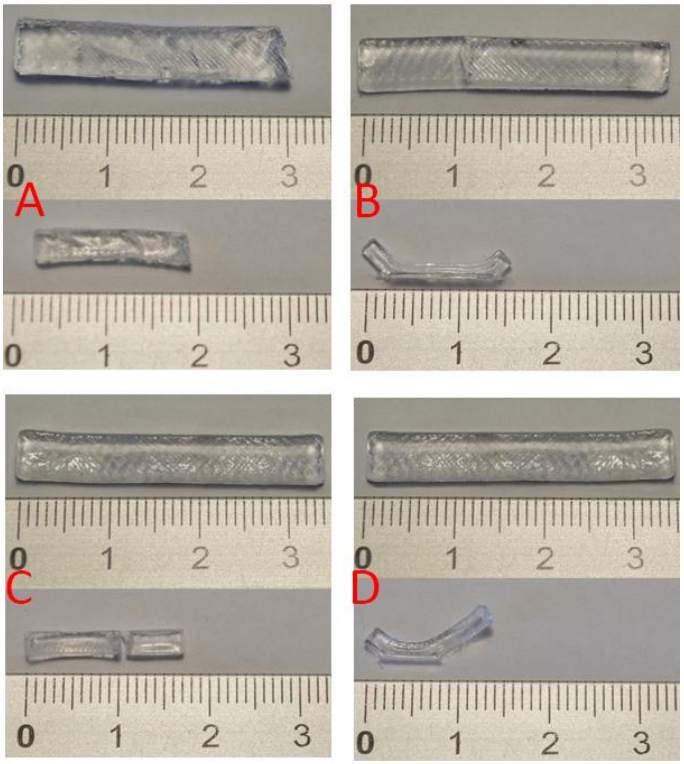

Fig.43: PAA samples at swelling equilibrium and completely dry. Their concentrations are A) 20%, B) 10%, C)7%, D)5%.

Variation in lenght was also measured, and we obtained

$$S_L\ \% = \frac{L_{swell} - L_{dry}}{L_{swell}} * 100$$

Where L_{swell} is the length of the sample at swelling equilibrium and L_{dry} is the length after the drying process described above. Most hydrogels are bent after the drying process, however they remain soft and flexible enough to be straightened.

Sample		S_W	S_L
PEGDA	60%	49.9%	30.1%
	30%	67.1%	41.4%
	20%	76%	63.2%
	10%	86.1%	72.1%
PAA	20%	82.1%	77.2%
	10%	88.5%	101.5%
	7%	93.4%	112.5%
	5%	94.4%	142.9%

Tab.5: Swelling of PEGDA and PAA.

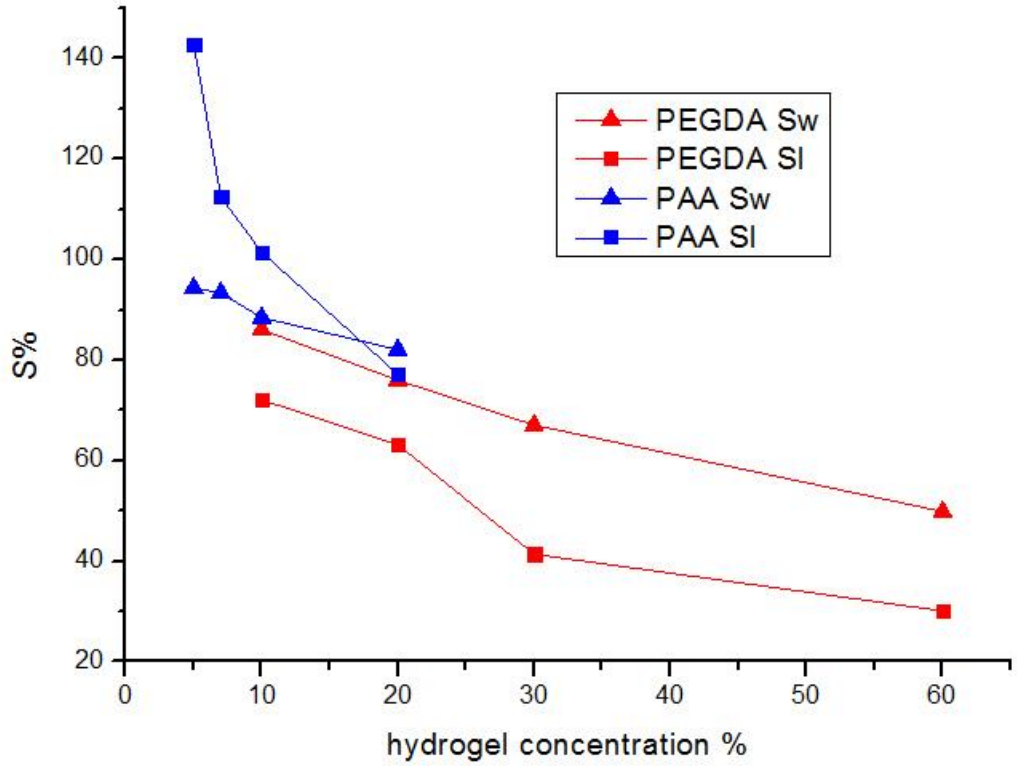

Fig.43: Swelling values of PEGDA and PAA depending on concentration.

4.2 Mechanical properties

As stated in the previous chapter, mechanical properties were tested via macroscopic compression, macroscopic indentation and microscopic indentation. The results obtained are shown in the table below:

Sample		Young's modulus [KPa]					
		Compression	**Error%**	**Indentation**	**Error%**	**AFM**	**Error%**
PEGDA	60%	1229.58	12.63	1229.27	1.44	813.81	8.47
	30%	500.23	19.82	533.45	19.66	58.39	40.63
	20%	195.67	17.93	206.60	5.02	3.18	27.11
	10%	69.33	25.41	75.23	3,71	0.71	20.52
PAA	20%	303.36	4.16	292.97	2.63	11.37	7.56
	10%	132.67	12.28	84.73	5.51	2.77	36.82
	7%	53.82	9.54	48.37	3.40	0.64	26.56
	5%	34.44	37.71	17.50	2.53	0.29	37.93

Tab.6: Young's modulus values of PEGDA and PAA for three different measurement: compression, macro indentation and micro indentation.

To check that thermal treatment time was long enough to achieve complete polymerisation of the hydrogels, PEGDA 60% and 30% and PAA 20% and 10% prepared in a smaller batch and were thermal treated three times longer the standard duration previously used for a given hydrogel. After this process they were measured by AFM and no significant difference from data obtained above were found.

Samples		Young's modulus [KPa]			
		Standard duration	Error%	Triple duration	Error%
PEGDA	60%	813.81	8.47	857.23	10.36
	30%	58.39	40.63	53.65	23.16
PAA	20%	11.37	7.56	11.32	8.81
	10%	2.77	36.82	2.89	40.11

Tab.7: Young's modulus values of PEGDA and PAA measured by AFM for samples after standard thermal treatment and triple duration termal treatment.

As can clearly be seen from the graph, the elastic modulus measured with macroscopic instrumentations gives almost the same values for PEGDA samples, and a very close, comparable result for PAA. However, the stiffness determined by the AFM differs increasingly from the those values the more diluted the hydrogel.

To understand this phenomenon we have to recall what has been said regarding poroelasticity: for a given sample of hydrogel which is under a load we have two forms of stress relaxation, the first involves movements of polymer chains and is defined only by the network conformation so that the relaxation time is independent from sample dimensions; the second one however is linked to the solvent migration inside or outside the hydrogel and is quadratic dependant to the distance that molecules have to travel before equilibrium is achieved. Since in the AFM test we are indenting 2-3 μm, opposed to the millimetre of the macro indentation, we hypothesize that the difference between the two set of data could lie in the different length that water have to migrate.

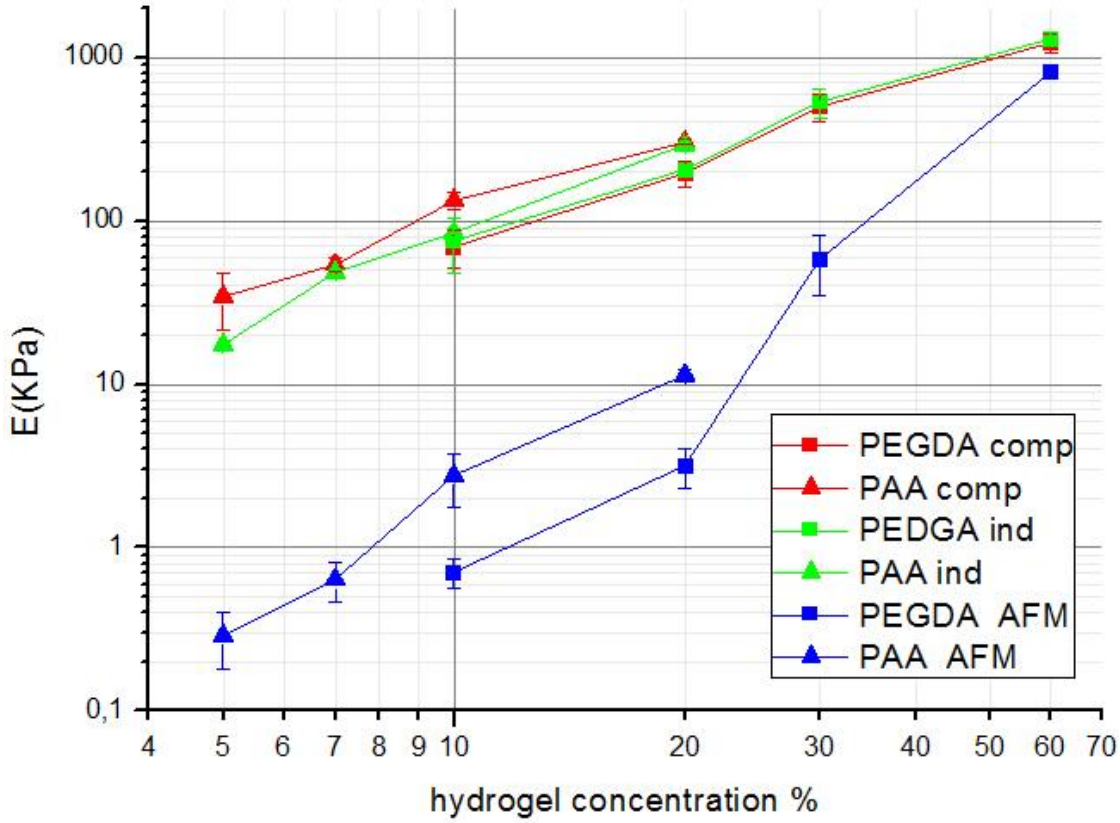

Fig.44: Mechanical properties of hydrogels tested with parallel plate compression (red) macro indentation (green) and micro indentation (blue).

To prove this, we measured the hydrogels' diffusion constant with a stress relaxation test: because the top and the bottom plates compressing the gel are impermeable, water can only migrate out of the disk from the edges, thus the radius of the disk is the only relevant length scale for the migration of water. Supposing the sample taken into account to be small enough so that we can consider the diffusion process predominant, the stress should take the following function

$$\sigma = F(\sqrt{t}/_R)$$

where σ is the stress, t is the time and R is the radius of the hydrogel disk. From this, we can approximate the diffusion constant to

$$D \approx R^2/_t$$

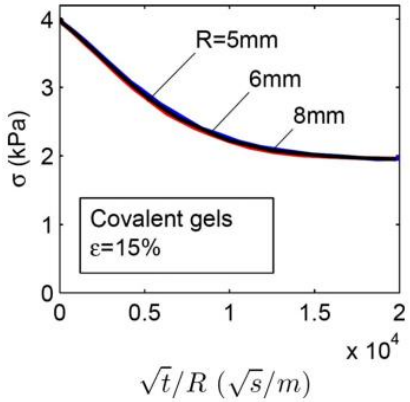

Fig.45: For different samples of the same hydrogel, when the stress is plotted as a function of $\sqrt{t}/R$ the curves for the disks of different radii collapse into a single curve [37].

and obtain the values reported below, which are comparable with data found in literature for PAA and PEGDA [42, 43].

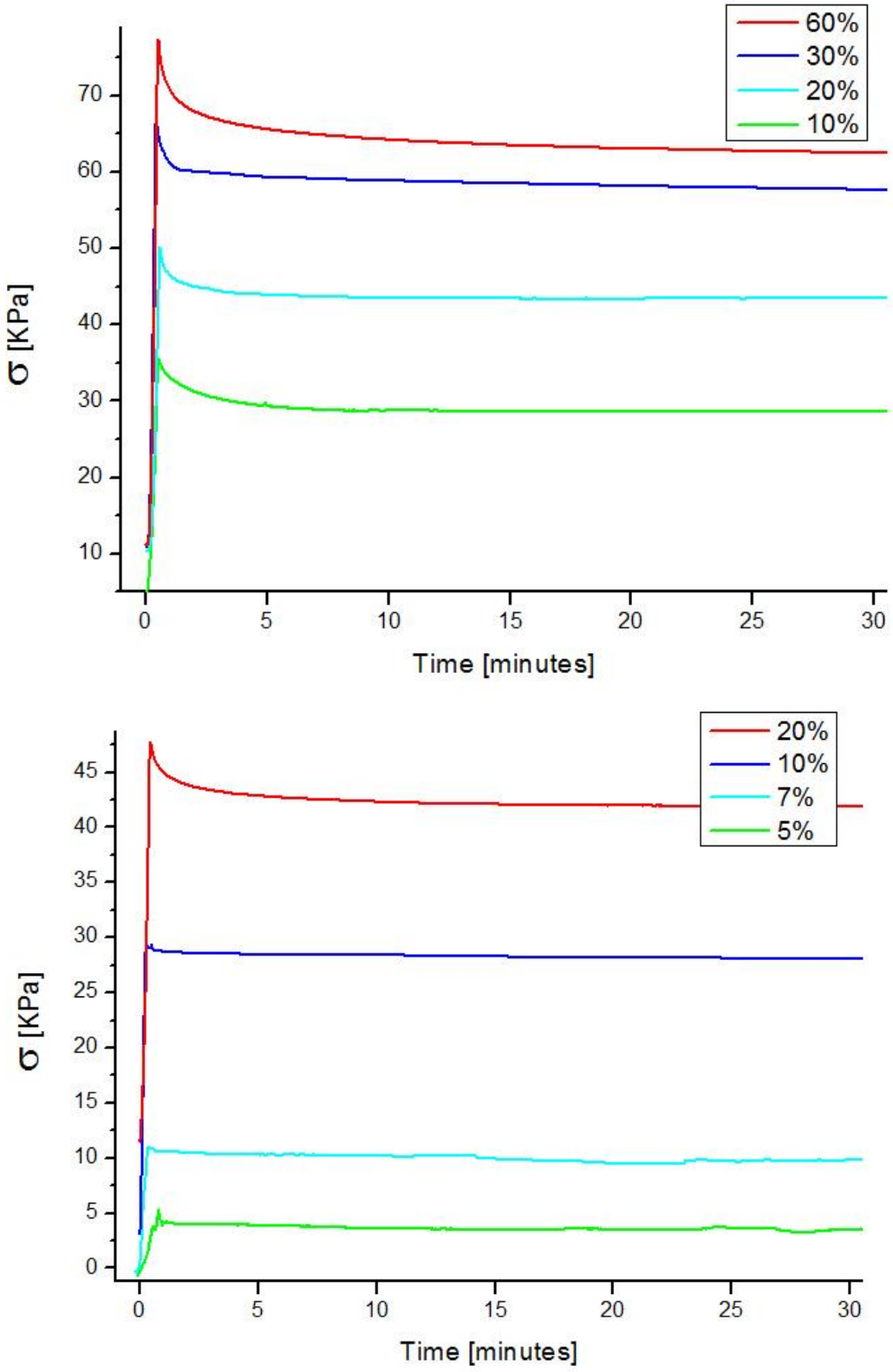

Fig.46: Stress relaxation test for PEGDA (left) and PAA (right); hydrogel were all compressed ≈ 2 mm and load was recorder for 30 min.

Sample		Relaxation Time [s]	R [mm]	D *10^{10} [m^2/s]
PEGDA	60%	6929	5.1	9.38
	30%	3757	5.1	17.43
	20%	1742	5.2	38.81
	10%	788	5	79.26
PAA	20%	15232	5	4.10
	10%	12317	4.9	4.87
	7%	3254	4.4	14.87
	5%	2243	4.8	25.68

Tab.8: Relaxation time from experimental interpolation, sample disk radius and diffusion constant for hydrogels with varying concentrations.

With this data, we can now estimate the time needed by hydrogels to relax under the load of the indentation: for a simplified approach, we will approximate the stress field from the complex profile of the Hertzian model to a constant σ_0 along the surface of the indenter; also the length of this field *d* will be proportional to the indentation depth *h*, so that $d = h$

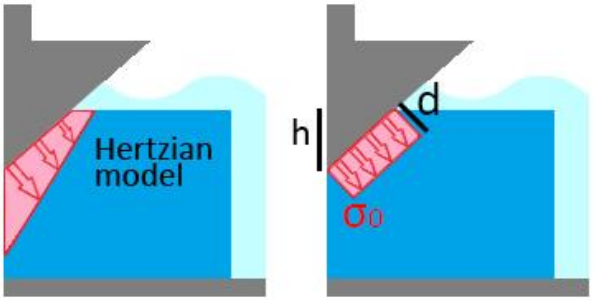

Fig.47: Approximation of the Hertzian model stress field to a constant field σ_0, *d* long, alongside the indenter surface.

Given this geometry, water will diffuse through a path which is 1 mm in the macro indentation, and 3 μm for the micro indentation. The time taken to complete this process is

$$t \approx d^2/D$$

so for every hydrogel we can see in the table below that for the macroscale we have a relaxation time which can be several order of magnitudes longer than the measurement time (≈1 s) while for the microscale is true the contrary since the test duration is about 10 s.
These results confirm our first hypothesis that in the micro indentation the stress relaxation phenomena is consistently present and causes the measurement of a relaxed elastic modulus, thus diverging from the macroscale values.

Samples		Macro indentation relaxation time [s]	Micro indentation relaxation time [s]
PEGDA	60%	1066	0.010
	30%	578	0.005
	20%	258	0.002
	10%	126	0.001
PAA	20%	2437	0.022
	10%	2052	0.018
	7%	672	0.006
	5%	389	0.004

Tab.9: Relaxation time for macro and micro indentation.

This hypothesis is also corroborated by AFM and macro indentations measurements done on a sample of PDMS with 10% crosslinker and cured at 100° for 45 min: this material was chosen because is not prone to adhesion and surface artefacts, being a relatively hard compared to hydrogels ; moreover since no solvent is present we can have only classic viscoelastic stress relaxation behaviour; in fact, in this case in fact both AFM and macro indentation gave the same value of ≈ 1MPa, in accordance with literature data [44].

4.3 Pillars replica

For the replica moulding process only hydrogels at the higher concentrations were employed since we needed the polymer to be strong enough not to break inside the silicon master. The pool setup described in the previous chapter proved to yield a better replica than the droplet setup, since in the second case we have smaller bubbles that do not coalesce and ultimately remains on the silicon surface causing defects. Both the master and the pillars dimensions were measured with a confocal microscope and are reported in the table below: several vacuum times were tested to achieve the maximum high in the replica, however it seems that it's not possible to completely fill the pillar cavity of the

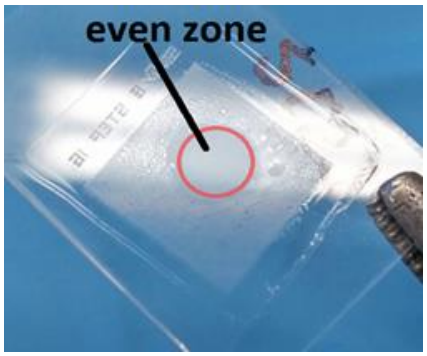

Fig.48: Pillars replica from droplet setup: we achieve an even replica only in the centre of the master, were bubbles could coalesce together more easily being in higher number, while peripherical areas are dotted in empty spaces.

master and keeping the sample under vacuum for more than 10 min did not affect the result significantly.

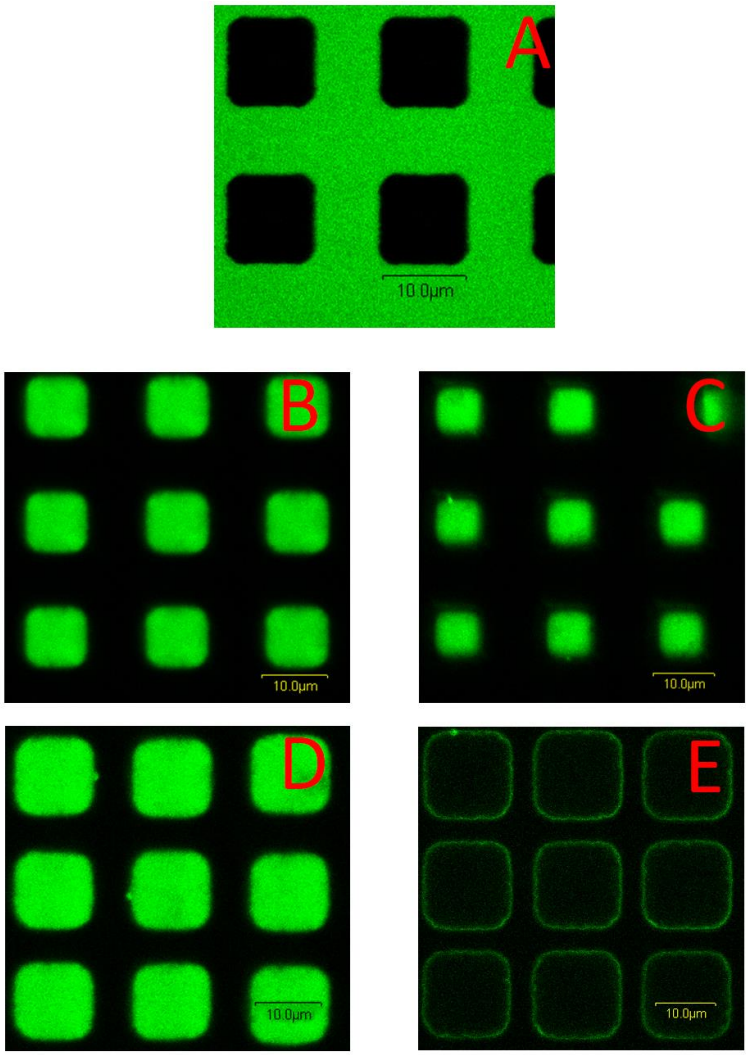

Fig.49: A) silicon master, B) PEGDA 60% pillars replica dry, C) AA 20% pillars dry, D) PEGDA 60% pillars replica after swelling in PBS medium and E) PAA 20% pillars replica after swelling in PBS medium.

Sample	Pillar width [µm]	Pillar high [µm]	Pillar separation [µm]
Silicon master	10.4	19	7.6
PEGDA 60% dry	9.8	15	8.2
PAA 20% dry	7.2	9	10.8
PEGDA 60% in medium	11.1	17	6.2
PAA 20% in medium	13.7	16.5	4.3

Tab.10: Silicon master and samples dimension.

We also tried to measure the Young's module of the pillars by probing the tip of the prism with the AFM indenter: unfortunately, due to the small length of the microstructure, resulting values were strongly perturbed by the glass substrate stiffness. We also tried to

probe the stiffness by bending the lateral side of the pillars, gluing the glass substrate perpendicular to the surface of the petri dish that contained the sample during the measure; in this case however it was not possible to locate properly the pillars and the indenter tip position, because subsequent rows to the one on the top being measured blocked the view of the inverse microscope that is mounted on the instrument, which is built to have an underside vision of the sample tested. Further optimisation of the setup will be necessary if we want to do this test.

To evaluate how much tall should be the pillars not to be affected by the substrate during stiffness tests, we prepared three films from PEGDA 60% of decreasing thickness: first a glass slide was functionalised with TMSPM to let the hydrogel adhere to it, while a second one was treated with ODTS to be used as cover during the heat treatment; to achieve the right spacing between the two several layers of biadhesive tape were arranged on the slide sides to a thickness of ≈40 μm, ≈160 μm, ≈300 μm and ≈1 mm.

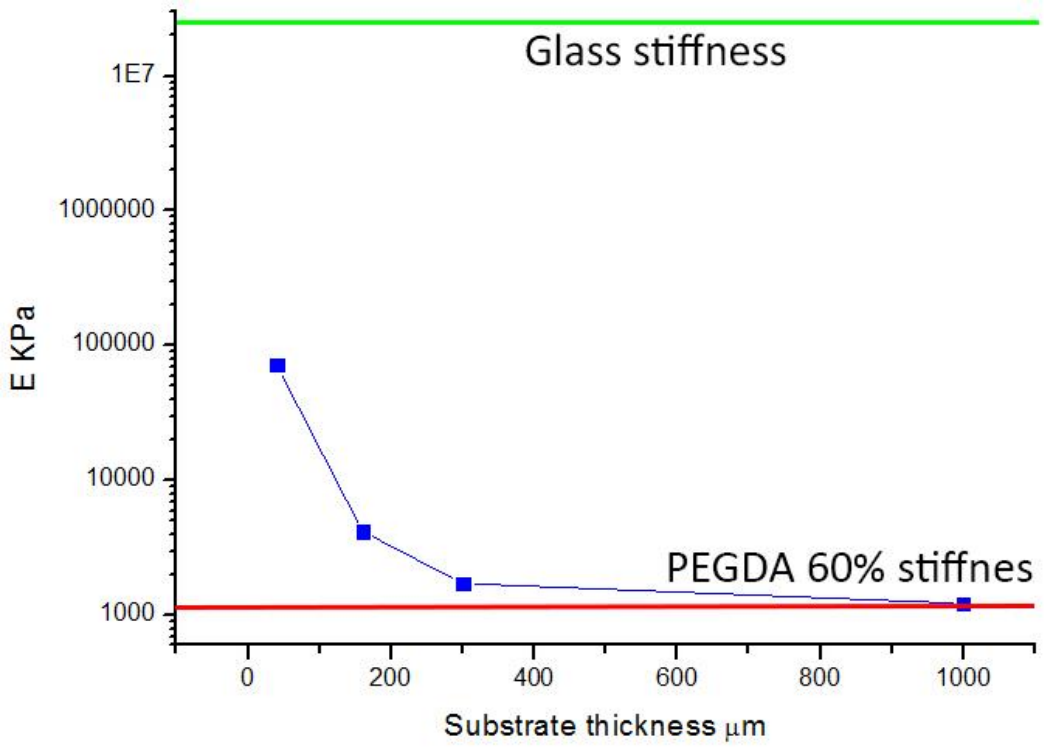

Fig.50: PEGDA 60% apparent stiffness for a film decreasing thickness over a glass substrate.

This test gives a minimum value of 1 mm, too high for the lateral dimension of the pillar we fabricated. Therefores the measure performed by bending the pillars would be needed which should not be affected by the substrate elastic modulus.

These substrates were employed to culture human embryonic stem cells: the aim of this was to see whether HESC nuclei can self-deform on hydrogel pillar substrates in the same way they do when cultured on hard-microstructured PDMS substrates, and in the future to develop pillars with correct stiffness in order to react and deform in correlation with change of nuclear stiffness, following cytoskeleton inhibition, cell differentiation, pathway activation etc.

The culture was carried out as follow:

1. 3 Acrylamide and 3 PEGDA hydrogel substrates where extensively rinsed in PBS overnight and then equilibrated/functionalized with DMEM f-12 with 2.5% matrigel reduced factor for 2 h in incubator.
2. HES2 p38 cells where detached from MEF and seeded in single cells on the substrates, and let adhere and expand for 48 h.
3. Cells and hydrogels where PFA fixed and stained for nuclei and actin filaments.

Cell successfully adhered on these substrates and HES2 seems to correctly deform between the pillars, even though after 2 days, colonies did not spread and grow enough, and this may be caused by low efficiency in hydrogel functionalization compared to plasma-treated PDMS. Actin seems not to be fully spread around the pillars, and also this may be caused by low efficiency in hydrogel functionalization.
Hydrogel pillars seem not to deform/bend when a cell falls between them, and this may be caused by high stiffness of the substrates; also, PEGDA pillars easily detach from glass bottom during pre-incubation/cell culture while PAA pillars are more stick to glass but 1 out of 3 substrates had the pillars completely collapsed.

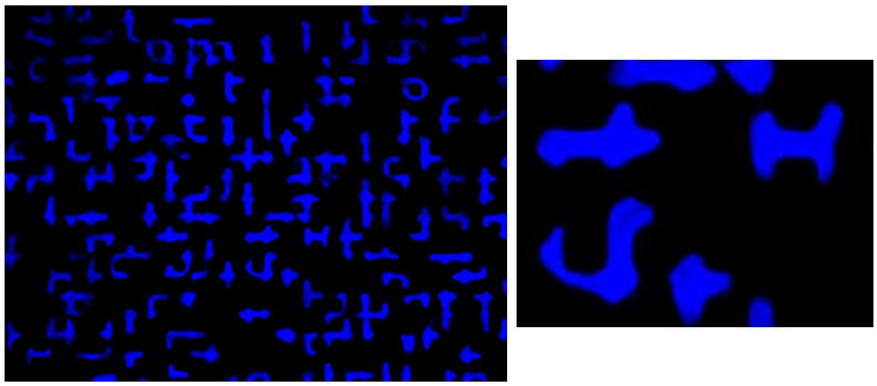

Fig.51: HES2 cell nuclei self-deform in PDMS microstructured substrates with pillars of 7x7x7 µm geometry.

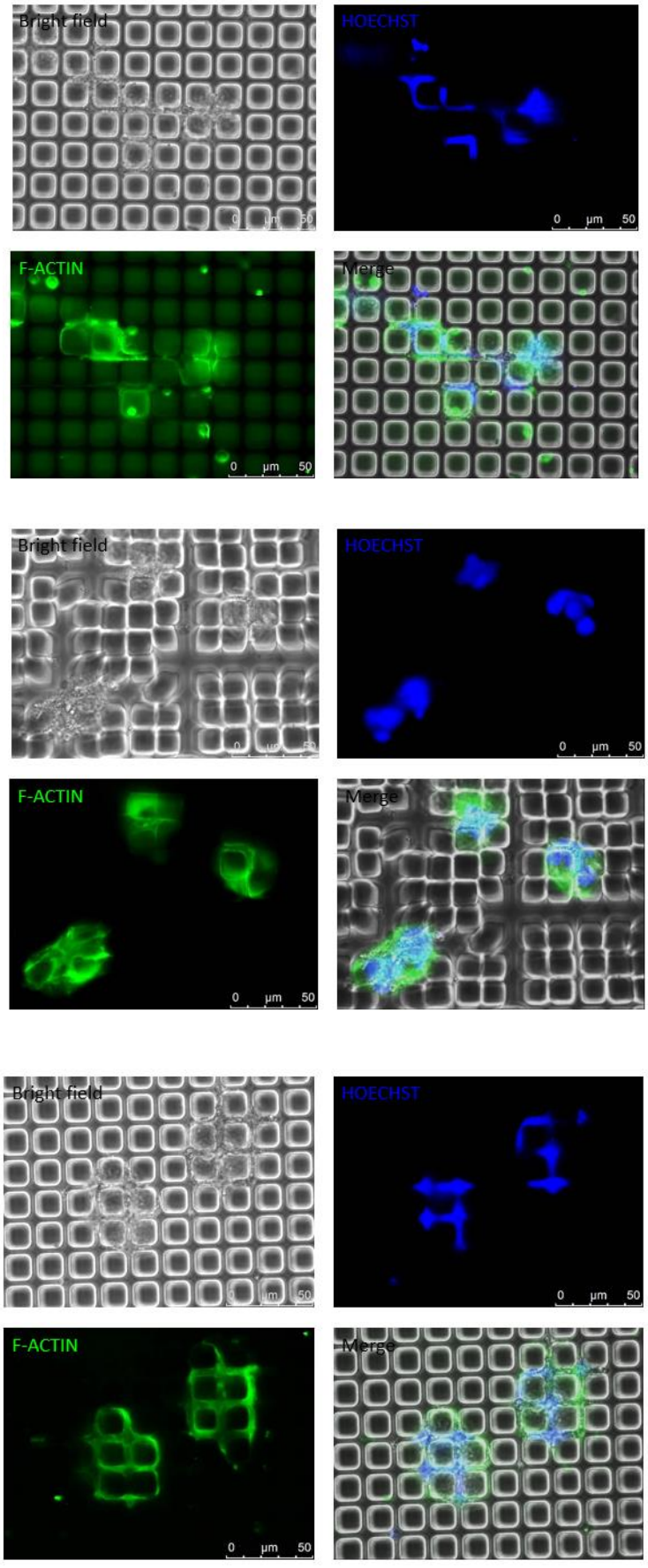

Fig.52: HES2 cell nuclei om PAA substrates

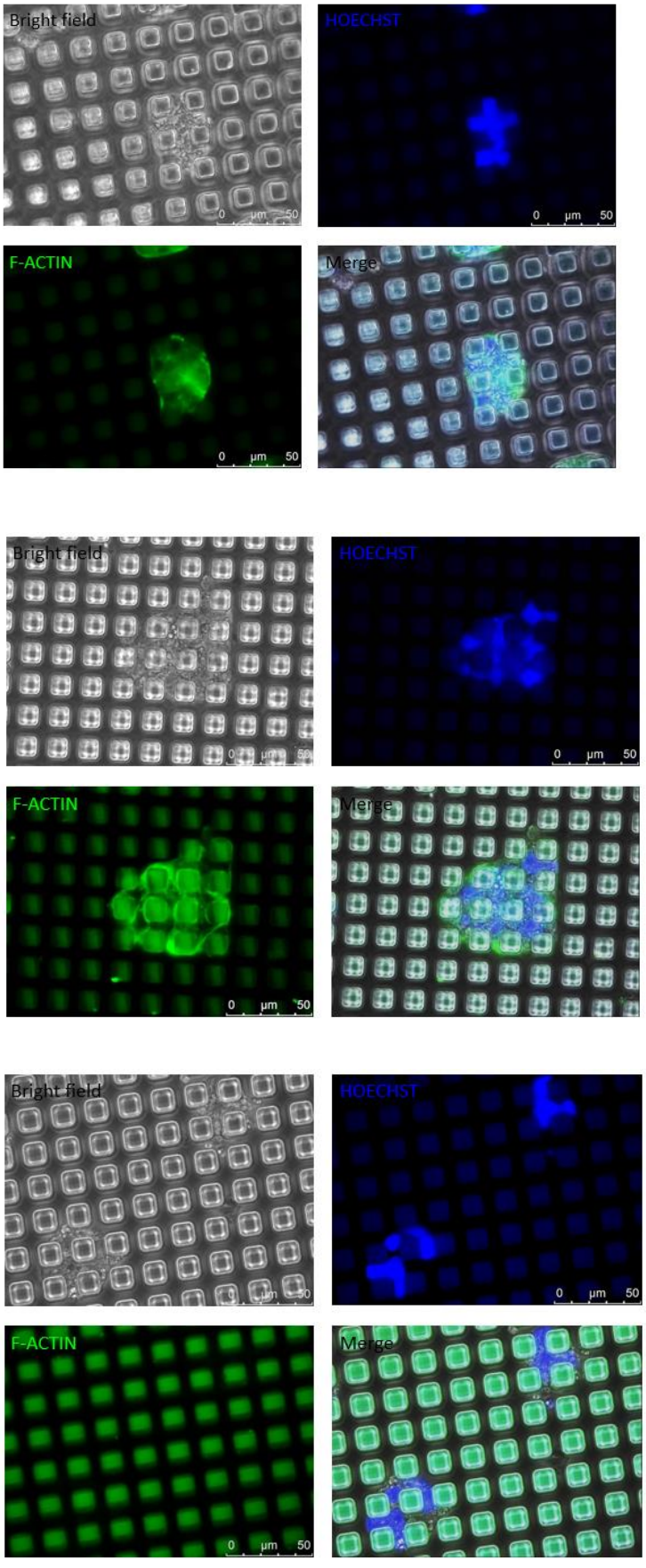

Fig.53: HES2 cell nuclei om PEGDA substrates

Chapter 5

Conclusions

Polyethilenglicoldiacrylate and acrylamide/bis-acrylamide were employed to synthetize hydrogels of varying concentration from 5% up to 60%; their mechanical properties were tested on bulk samples in three manners: compression between two plates, macro indentation with a spherical indenter and micro indentation with pyramidal indenter. While compression and macro indentation gave very similar results, we observed an increasing discrepancy between these and micro indentation values, growing larger with higher water content: this difference was proven to be caused by stress relaxation phenomena which in hydrogel are due to both network chains movement and water migration from loaded to non-loaded regions. By calculating the diffusion constant for every sample, we managed to evaluate the time needed for the hydrogel to relax in the macro and micro indentation tests and found that while in the macroscale the measure duration is 2-3 orders of magnitude smaller than the relaxation time, in the microscale hydrogels relaxation time is 3-4 orders of magnitude smaller than the measure duration. This means that AFM determines a relaxed Young modulus, while compression and macro indentation give an unrelaxed and stiffer value.

These hydrogels were also employed to fabricate micro structured substrate for human embryonic stem cells culture: while cell adhesion and deformation occurred as expected, cells spreading and growth were unsatisfactory and this may be due to low efficiency in hydrogel functionalization.
Also, pillars were expected to bend but it seems that the hydrogels employed are too stiff compared to the force exercised by stem cells.

Bibliography

1. Kristi S. Anseth et al., Mechanical properties of hydrogels and their experimental determination, *Biomat.*, 1996, **17** 1647-1657
2. Enas M. Ahmed, Hydrogel: Preparation, characterization, and applications: A review, *Journal of Advanced Research,* 2015, **6**, 105–121
3. Kazutoshi Haraguchi et al., Compositional Effects on Mechanical Properties of Nanocomposite Hydrogels Composed of Poly(N,N-dimethylacrylamide) and Clay, *Macromolecules*, 2003, **36**, 5732-5741
4. Kuen Yong Lee et al., Controlling Mechanical and Swelling Properties of Alginate Hydrogels Independently by Cross-Linker Type and Cross-Linking Density, *Macromolecules* , 2000, **33**, 4291-4294
5. Oded Pinkas et al., Fiber-reinforced composite hydrogels for bioadhesive and sealant applications, *Wiley Online Library* 2017
6. Petra Eiselt et al., Rigidity of Two-Component Hydrogels Prepared from Alginate and Poly(ethylene glycol)-Diamines, *Macromolecule*s 1999, **32**, 5561-5566
7. Jeannine E. Elliott et al., Structure and swelling of poly(acrylic acid) hydrogels: effect of pH, ionic strength, and dilution on the crosslinked polymer structure, *Polymer*, 2004, **45,** 1503–1510
8. Esmaiel Jabbari, Samyra Nozari, Swelling behavior of acrylic acid hydrogels prepared by c-radiation crosslinking of polyacrylic acid in aqueous solution, *European Polymer Journal*, 2000, **36** 2685–2692
9. J. Berger et al., Structure and interactions in covalently and ionically crosslinked chitosan hydrogels for biomedical applications, European Journal of *Pharmaceutics and Biopharmaceutics*, 2004, **57** 19–34
10. A. Martı ´nez-Ruvalcaba et al, Viscoelastic properties of dispersed chitosan/xanthan hydrogels, *Carbohydrate Polymers*, 2007, **67** 586–595
11. E. Vallés et al, Equilibrium swelling and mechanical properties of hydrogels of acrylamide and itaconic acid or its esters, *Polymer Bulletin*, 2000, **44**, 109–114
12. Jason A. Stammen et al., Mechanical properties of a novel PVA hydrogel in shear and unconfned compression, *Biomaterials*, 2001, **22** 799-806
13. Uday Chippada et al., Simultaneous determination of Young's modulus, shear modulus, and Poisson's ratio of soft hydrogels, 2009
14. Sheng Lin-Gibson et al., Structure-Property Relationships of Photopolymerizable Poly(ethyleneglycol) Dimethacrylate Hydrogels, *Macromolecules*, 2005, **38**, 2897-2902
15. Huimin Liao et al., Influence of hydrogel mechanical properties and mesh size on vocal fold fibroblast extracellular matrix production and phenotype, Acta *Biomaterialia*, 2008, **4** 1161–1171

16. Jia Ban Toh, Synthesis and Characterisation of PEGDAbased Hydrogels, PhD thesis, School of Materials Science & Engineering 2011
17. Robert J. Pelham, Yu-Li Wang, Cell locomotion and focal adhesions are regulated by substrate flexibility, *Proc. Natl. Acad. Sci. USA*, 1997, **Vol. 94**, pp. 13661–13665
18. Mark Ahearne et al., Characterizing the viscoelastic properties of thin hydrogel-based constructs for tissue engineering applications, *Interface* 2005, **2**, 455-463
19. Robert J. Pelham, Yu-Li Wang, Cell locomotion and focal adhesions are regulated by substrate flexibility, *Proc. Natl. Acad. Sci. USA*, 1997, **Vol. 94**, pp. 13661–13665
20. Jeanie L. Drury et al., The tensile properties of alginate hydrogels, *Biomaterials*, 2004, **25**, 3187–3199
21. Guoqing Jiang et al., Network structure and compositional effects on tensile mechanical propertiesof hydrophobic association hydrogels with high mechanical strength, *Polymer*, 2010 , **51** 1507–1515
22. Mary c. Boyce, Ellen M Arruda, CONSTITUTIVE MODELS OF RUBBER ELASTICITY:A REVIEW
23. J.-S. Park et al., Thermal and dynamic mechanical analysis of PVA/MC blend hydrogels, *Polymer*, 2001, **42** 4271–4280
24. Stefan Gäbler et al., Determination of the viscoelastic properties of hydrogels based on polyethylene glycol diacrylate (PEG-DA) and human articular cartilage, *Int. J. Materials Engineering Innovation*, 2009, **Vol. 1**, No. 1
25. Clayton T. McKee et al., Indentation Versus Tensile Measurements of Young's Modulus for Soft Biological Tissues, *TISSUE ENGINEERING: Part B*, 2011, **Volume 17**, Number 3
26. XEI software manual, version 1.8.0, 2011, Park System corporation
27. Eric M. Darling et al., Spatial Mapping of the Biomechanical Properties of the Pericellular Matrix of Articular Cartilage Measured In Situ via Atomic Force Microscopy, *Biophysical Journal*, 2010, **Volume 98**
28. Jing Song et al., Contact Mechanics of UV/Ozone-Treated PDMS by AFM and JKR Testing: Mechanical Performance from Nano- to Micrometer Length Scales, *Macromolecules*, 2008, **41**, 6757-6762
29. Raimon Sunyer et al., Fabrication of Hydrogels with Steep Stiffness Gradients for Studying Cell Mechanical Response, *PLOS ONE*, 2012, **Volume 7**, Issue 10 e46107
30. Justin R. Tse, Adam J. Engler, Stiffness Gradients Mimicking In Vivo Tissue Variation Regulate Mesenchymal Stem Cell Fate, *PLOS ONE*, 2011, **Volume 6**, Issue 1 e15978
31. Alastair Selby et al., Influence of specimen thickness on the nanoindentation of hydrogels: Measuring the mechanical properties of soft contact lenses, J*ournal of the mechanical behavior of biomedical materials*, 2014, **35** 144 – 156
32. Joe Swift et al., Nuclear Lamin-A Scales with Tissue Stiffness and Enhances Matrix-Directed Differentiation, *Science*, 2014, **341**, 1240104

33. Adam J. Engler et al., Matrix Elasticity Directs Stem Cell Lineage Specification, *Cell*, 2006, **126**, 677–689
34. Matthew J. Paszek et al., Tensional homeostasis and the malignant phenotype, *Cancer cell*, 2005, **VOL. 8**
35. Sirio Dupont et al., Role of YAP/TAZ in mechanotransduction, *Nature*, 2011, **vol. 474**
36. Zouheir Drira, Vamsi K. Yadavalli, Nanomechanical measurements of polyethylene glycol hydrogels using atomic force microscopy, J*ournal of the mechanical behavior of biomedical materials*, 2013, **18** 20-28
37. Xuanhe Zhao et al., Stress-relaxation behavior in gels with ionic and covalent crosslinks, *Journal of Applied Physics*, 2010, **107**
38. Yuhang Hu et al, Indentation: A simple, nondestructive method for characterizing the mechanical and transport properties of pH-sensitive hydrogels, *Res.*, 2011, **Vol. 27**, 153
39. Yuhang Hu et al., Using indentation to characterize the poroelasticity of gels, *Applied Physics Letters*, 2010, **96**
40. Edwin P. Chan et al., Poroelastic relaxation of polymer-loaded hydrogels, Soft Matter, 2012, 8, 8234
41. Justin R. Tse, Adam J. Engler, Preparation of Hydrogel Substrates with Tunable Mechanical Properties, *Current Protocols in Cell Biology*, 2010
42. Chaenyung Cha, Tuning the dependency between stiffness and permeability of a cell encapsulating hydrogel with hydrophilic pendant chains, *Acta Biomaterialia*, 2011, **7** 3719–3728
43. W. Brown, R. M. Johnsen, Diffusion in polyacrylamide gels, *POLYMER*,1981, **Vol 22**, Februar
44. Nicholas D. Evans et al., SUBSTRATE STIFFNESS AFFECTS EARLY DIFFERENTIATION EVENTS IN EMBRYONIC STEM CELLS, *European Cells and Materials*, 2009, **Vol. 18** pag. 1-14

Acknowledgement

Per questa tesi voglio ringraziare il Prof. Alessandro Martucci e il Dott. Marco Angiola per l'opportunità di studio in quest'ambito di ricerca e per la disponibilità dimostrata lungo tutto lo svolgersi di questo lavoro.

Ringrazio inoltre tutti i compagni di laboratorio, e in particolare il Dott. Tommaso Bressan, per l'aiuto e i consigli che hanno contribuito all'esito della mia esperienza.

Un ringraziamento speciale va ai miei colleghi Francesco Monni e Giulia Venturato, per la pazienza e l'aiuto in tutti i problemi ,burocratici e non, che sono sorti lungo il tragitto.

Infine, ringrazio i miei genitori, grazie ai quali mi è stato possibile intraprendere questo percorso, per il loro sostegno e per la loro presenza.